HAL
open science

A DDR method for the Reissner-Mindlin plate bending problem on polygonal meshes

Daniele Antonio Di Pietro, Jérôme Droniou

To cite this version:

Daniele Antonio Di Pietro, Jérôme Droniou. A DDR method for the Reissner-Mindlin plate bending problem on polygonal meshes. 2021. hal-03234088

HAL Id: hal-03234088

https://hal.science/hal-03234088

Preprint submitted on 25 May 2021

HAL is a multi-disciplinary open access archive for the deposit and dissemination of scientific research documents, whether they are published or not. The documents may come from teaching and research institutions in France or abroad, or from public or private research centers.

L'archive ouverte pluridisciplinaire **HAL**, est destinée au dépôt et à la diffusion de documents scientifiques de niveau recherche, publiés ou non, émanant des établissements d'enseignement et de recherche français ou étrangers, des laboratoires publics ou privés.

A DDR method for the Reissner–Mindlin plate bending problem on polygonal meshes

Daniele A. Di Pietro[1] and Jérôme Droniou[2]

[1]IMAG, Univ Montpellier, CNRS, Montpellier, France, daniele.di-pietro@umontpellier.fr
[2]School of Mathematics, Monash University, Melbourne, Australia, jerome.droniou@monash.edu

May 25, 2021

Abstract

In this work we propose a discretisation method for the Reissner–Mindlin plate bending problem in primitive variables that supports general polygonal meshes and arbitrary order. The method is inspired by a two-dimensional discrete de Rham complex for which key commutation properties hold that enable the cancellation of the contribution to the error linked to the enforcement of the Kirchhoff constraint. Denoting by $k \geq 0$ the polynomial degree for the discrete spaces and by h the meshsize, we derive for the proposed method an error estimate in h^{k+1} for general k, as well as a locking-free error estimate for the lowest-order case $k = 0$. The theoretical results are validated on a complete panel of numerical tests.

Key words. Reissner–Mindlin plates, discrete de Rham complex, locking free method, compatible discretisations, polygonal methods

MSC2010. 65N30, 65N12, 74K20, 74S05, 65N15

1 Introduction

In this work we propose a novel discretisation method for the Reissner–Mindlin plate bending problem in primitive variables that supports general polygonal meshes and arbitrary order. In its lowest-order version, the method can be proved to behave robustly with respect to the plate thickness t. Its design is based on the two-dimensional discrete de Rham (DDR) complex of [19], for which key commutation properties hold that enable the cancellation of the contribution to the error linked to the enforcement of the Kirchhoff constraint.

We consider in what follows an elastic plate of thickness $t > 0$ with reference configuration $\Omega \times \left(-\frac{t}{2}, \frac{t}{2}\right)$, where $\Omega \subset \mathbb{R}^2$ is a bounded connected polygonal domain with boundary $\partial\Omega$. Without loss of generality, it is assumed in what follows that Ω has diameter 1 and that $t < 1$. The Reissner–Mindlin model describes the deformation of the plate in terms of the rotation $\boldsymbol{\theta} : \Omega \to \mathbb{R}^2$ of the fibers initially perpendicular to its midsurface and of the transverse displacement $u : \Omega \to \mathbb{R}$. Introducing the shear strain $\boldsymbol{\gamma}$ and denoting by $f : \Omega \to \mathbb{R}$ the transverse load, the strong formulation of the model with clamped boundary conditions reads

$$\boldsymbol{\gamma} + \mathbf{div}(\mathbf{C}\,\mathbf{grad}_{\mathrm{s}}\,\boldsymbol{\theta}) = \mathbf{0} \qquad \text{in } \Omega, \tag{1a}$$

$$-\operatorname{div}\boldsymbol{\gamma} = f \qquad \text{in } \Omega, \tag{1b}$$

$$\boldsymbol{\gamma} = \frac{\kappa}{t^2}(\mathbf{grad}\,u - \boldsymbol{\theta}) \qquad \text{in } \Omega, \tag{1c}$$

$$\boldsymbol{\theta} = \mathbf{0}, \quad u = 0 \qquad \text{on } \partial\Omega. \tag{1d}$$

Here, **div** is the row-wise divergence of tensors, $\mathbf{grad}_{\mathrm{s}}$ is the symmetric part of the gradient applied to vector-valued fields over Ω, and $\mathbf{C}$ is the fourth-order tensor defined by $\mathbf{C}\mathbf{t} = \beta_0\mathbf{t} + \beta_1(\operatorname{tr}\mathbf{t})\mathbf{I}$ for all second-order tensor $\mathbf{t}$, with $\mathbf{I}$ the identity tensor. The parameters of $\mathbf{C}$ are $\beta_0 := \frac{E}{12(1+\nu)}$ and $\beta_1 := \frac{E\nu}{12(1-\nu^2)}$, where $E > 0$ and $\nu \in [0, \frac{1}{2})$ are the Young modulus and Poisson ratio of the material, respectively. The shear modulus κ is given as $\kappa := \frac{\kappa_0 E}{2(1+\nu)}$, with shear correction factor κ_0 usually taken equal to $\frac{5}{6}$ for clamped plates. Denoting by $H^1_0(\Omega)$ the space of real-valued functions that are square-integrable along with their derivatives and that vanish on $\partial\Omega$ in the sense of traces, the standard weak formulation of (1) hinges on the spaces $\mathbf{\Theta} := H^1_0(\Omega)^2$ for the rotation and $U := H^1_0(\Omega)$ for the transverse displacement. Specifically, assuming that $f \in L^2(\Omega)$, it reads: Find $(\boldsymbol{\theta}, u) \in \mathbf{\Theta} \times U$ such that

$$A((\boldsymbol{\theta}, u), (\boldsymbol{\eta}, v)) = \ell(v) \qquad \forall (\boldsymbol{\eta}, v) \in \mathbf{\Theta} \times U, \tag{2}$$

where the bilinear form $A : [\mathbf{\Theta} \times U]^2 \to \mathbb{R}$ and the linear form $\ell : U \to \mathbb{R}$ are such that, for all $(\boldsymbol{\tau}, w), (\boldsymbol{\eta}, v) \in \mathbf{\Theta} \times U$,

$$A((\boldsymbol{\tau}, w), (\boldsymbol{\eta}, v)) := a(\boldsymbol{\tau}, \boldsymbol{\eta}) + b((\boldsymbol{\tau}, w), (\boldsymbol{\eta}, v)), \qquad \ell(v) := \int_\Omega f v,$$

with bilinear forms $a : \mathbf{\Theta} \times \mathbf{\Theta} \to \mathbb{R}$ and $b : [\mathbf{\Theta} \times U]^2 \to \mathbb{R}$ such that

$$a(\boldsymbol{\tau}, \boldsymbol{\eta}) := \beta_0 \int_\Omega \mathbf{grad}_{\mathrm{s}}\, \boldsymbol{\tau} : \mathbf{grad}_{\mathrm{s}}\, \boldsymbol{\eta} + \beta_1 \int_\Omega \operatorname{div} \boldsymbol{\tau}\ \operatorname{div} \boldsymbol{\eta}, \tag{3}$$

$$b((\boldsymbol{\tau}, w), (\boldsymbol{\eta}, v)) := \frac{\kappa}{t^2} \int_\Omega (\boldsymbol{\tau} - \mathbf{grad}\, w) \cdot (\boldsymbol{\eta} - \mathbf{grad}\, v). \tag{4}$$

The role of the bilinear form b is to enforce the Kirchhoff constraint that, as $t \to 0$, the rotation of the normal fibers equals the gradient of the transverse displacement. Notice that the choice of considering clamped boundary conditions is made for the sole purpose of simplifying the theoretical discussion: other standard boundary conditions can be considered with straightforward modifications. A critical point in the numerical approximation of problem (2) is robustness for small t. Methods for which error estimates uniform in t can be established are commonly referred to as (shear) *locking-free*.

The finite element literature for the locking-free discretisation of problem (2) on standard meshes dates back to the 1980s. In [15], the authors proposed a reformulation involving, in addition to the primitive variables $\boldsymbol{\theta}$ and u, the introduction of two additional variables corresponding to the irrotational and solenoidal parts of the transverse shear strain. This work pointed out the relevance of establishing a discrete version of the Helmholtz decomposition to obtain error estimates uniform in t. A method in primitive variables was later proposed in [5], based on a nonconforming (Crouzeix–Raviart) piecewise linear space for the displacement and a bubble-enriched continuous space for the rotation, and involving a projection in the discrete version of the bilinear form b. Recent developments of these ideas, including the extension to higher orders and the use of the Taylor–Hood element pair for the underlying Stokes problem, can be found in [25, 30] The idea of using reduced integration or projections in the enforcement of the Kirchhoff constraint can be found in several other works; see, e.g., [6, 16, 24, 27, 29]. A different approach, resorting to a mixed formulation where the shear strain appears as a separate unknown, is considered in [2]. The key point is, in this case, the design of a suitable coupling bilinear form, for which abstract conditions are provided. Recent results on mixed finite element schemes can be found in [26]; see also the references therein. Mixed approaches inspired by fully nonconforming (discontinuous Galerkin) methods have been proposed in [4], later leading to choices of finite element spaces that do not require reduced integration [3]; see also [17, 28] for related developments. Discontinuous Galerkin methods in their weakly over-penalised symmetric formulation are considered in [13, 14].

While the use of standard (e.g., simplicial conforming) meshes can be satisfactory for simple geometries and problems, it may lack flexibility in more complex situations. The support of general

meshes can greatly simplify the meshing process in the presence of small geometric features [1] and pave the way for advanced techniques such as nonconforming adaptive mesh refinement (which does not trade mesh quality for size) and mesh coarsening [7, 8, 22], that are crucial to exploit high-order approximation in the presence of geometric singularities. Owing to the onset of polygonal elements and/or hanging nodes, such strategies are inaccessible to standard conforming finite elements. These and similar considerations have prompted, in the last few years, the development of locking-free discretisation methods for problem (2) supporting general polygonal meshes. A first example is provided by the low-order Mimetic Finite Difference method of [10], that hinges on transverse displacements defined at mesh vertices, rotations defined at mesh vertices and edges, and uses shear forces at edges as intermediate unknowns. The key ingredient to establish a first-order locking-free error estimate is once again a discrete Helmholtz decomposition. A lowest-order Virtual Element method has also been recently proposed in [11], inspired by the reformulation of problem (2) originally introduced in [9] in the context of Isogeometric Analysis and using the transverse displacement and shear strain as unknowns.

The DDR method proposed in this work contains several key elements of novelty. First, to the best of our knowledge, it is the first scheme to support general polygonal meshes and high-order. Second, it does not resort to reduced integration or projections in the discrete counterpart of the bilinear form b. Third, it admits an inexpensive lowest-order version for which locking-free estimates can be rigorously established. The starting point for the design of the scheme is the two-dimensional DDR complex of [19, Remark 13]. This complex satisfies a crucial commutation property between the reconstructions of the discrete displacement gradient, the continuous gradient, and the interpolators on the corresponding spaces; see (10) below. When performing a convergence analysis in the spirit of the Third Strang Lemma [18], one can leverage this commutation property to cancel the error resulting from the enforcement of the Kirchhoff constraint through the discrete counterpart of the bilinear form b. This remark suggests the use of DDR counterparts of the $H^1_0(\Omega)$ and $\boldsymbol{H}_0(\mathrm{rot};\Omega)$ spaces for the displacement and the rotation, respectively. In order to have sufficient information to reconstruct a full strain tensor, the discrete $\boldsymbol{H}_0(\mathrm{rot};\Omega)$ space has to be enriched by the addition of normal components at edges. It turns out that this enriched space can be embedded into the standard Hybrid High-Order (HHO) space for elasticity originally introduced in [21] (see also [20, Chapter 7] and [12] for an application of HHO methods to Kirchhoff–Love plates), so that the standard HHO construction can be exploited to design the discrete counterpart of the bilinear form a. With these ingredients, we establish in Theorem 4 an estimate in h^{k+1} (with h denoting the meshsize and k the polynomial degree of the DDR sequence) for the natural (coercivity) norm of the error. The right-hand side of this estimate does not explicitly depend on t, but involves, as is unavoidable for high-order schemes, norms of higher order derivatives of the strain; such norms are not expected to remain bounded as $t \to 0$. Through the introduction of novel liftings of the displacement and of the rotation, we show in Theorem 6 that an error estimate uniform in t (and thus locking-free) can be established in the lowest order case $k = 0$.

The rest of the paper is organised as follows. In Section 2 we introduce the discrete setting. Section 3 contains the statement of the discrete problem preceeded by the required constructions. The analysis of the method is carried out in Section 4, the main theorems being stated in Section 4.2 and their proofs given in Sections 4.3 and 4.4. Finally, Section 5 contains a complete panel of numerical results, introducing a novel analytical solution for the model and showing that the method displays, to a certain extent, a locking-free behaviour also for $k \geq 1$.

2 Setting

2.1 Mesh

For any measurable set $Y \subset \mathbb{R}^2$, we denote by $h_Y := \sup\{|\boldsymbol{x} - \boldsymbol{y}| \,:\, \boldsymbol{x}, \boldsymbol{y} \in Y\}$ its diameter and by $|Y|$ its Hausdorff measure. We consider meshes $\mathcal{M}_h := \mathcal{T}_h \cup \mathcal{E}_h \cup \mathcal{V}_h$, where: $\mathcal{T}_h$ is a finite collection of open disjoint polygonal elements such that $\overline{\Omega} = \bigcup_{T \in \mathcal{T}_h} \overline{T}$ and $h = \max_{T \in \mathcal{T}_h} h_T > 0$; $\mathcal{E}_h$ is the set collecting

the open polygonal edges (line segments) of the elements; $\mathcal{V}_h$ is the set collecting the edge endpoints. It is assumed, in what follows, that $(\mathcal{T}_h, \mathcal{E}_h)$ matches the conditions in [20, Assumption 7.6]. The sets collecting the mesh edges that lie on the boundary of a mesh element $T \in \mathcal{T}_h$ and on $\partial\Omega$ are denoted by $\mathcal{E}_T$ and $\mathcal{E}_h^{\mathrm{b}}$, respectively. We also denote by $\mathcal{E}_h^{\mathrm{i}} = \mathcal{E}_h \setminus \mathcal{E}_h^{\mathrm{b}}$ the set of internal edges. The coordinates vector of $V \in \mathcal{V}_h$ is denoted by $\boldsymbol{x}_V$.

Each $E \in \mathcal{E}_h$ is endowed with an orientation determined by a fixed unit tangent vector $\boldsymbol{t}_E$; we then choose the unit normal $\boldsymbol{n}_E$ such that $(\boldsymbol{t}_E, \boldsymbol{n}_E)$ forms a right-hand system of coordinates. For $T \in \mathcal{T}_h$ and $E \in \mathcal{E}_T$, we set $\omega_{TE} = 1$ if $\boldsymbol{t}_E$ points in the clockwise direction of ∂T, and $\omega_{TE} = -1$ otherwise. It can be checked that $\boldsymbol{n}_{TE} := \omega_{TE}\boldsymbol{n}_E$ is the outer unit normal to T on E.

2.2 Polynomial spaces

For any $Y \in \mathcal{T}_h \cup \mathcal{E}_h$, we denote by $\mathcal{P}^\ell(Y)$ the space spanned by the restriction to Y of two-variate polynomials of total degree $\leq \ell$, with the convention that $\mathcal{P}^{-1}(Y) = \{0\}$. We additionally denote by $\pi^\ell_{\mathcal{P},Y}$ the corresponding L^2-orthogonal projector. For all $E \in \mathcal{E}_h$, the space $\mathcal{P}^\ell(E)$ is isomorphic to univariate polynomials of total degree $\leq \ell$ (see [20, Proposition 1.23]). In what follows, with a little abuse of notation, both spaces are denoted by $\mathcal{P}^\ell(E)$. For $Y \in \mathcal{T}_h \cup \mathcal{E}_h$, the vector and tensor versions of $\mathcal{P}^\ell(Y)$ are respectively denoted by $\boldsymbol{\mathcal{P}}^\ell(Y) := \mathcal{P}^\ell(Y)^2$ and $\mathbf{P}^\ell(Y) := \mathcal{P}^\ell(Y)^{2\times 2}$, and the corresponding L^2-orthogonal projectors $\boldsymbol{\pi}^\ell_{\boldsymbol{\mathcal{P}},Y}$ and $\boldsymbol{\pi}^\ell_{\mathbf{P},Y}$ are obtained applying $\pi^\ell_{\mathcal{P},Y}$ component-wise. We additionally denote by $\mathbf{P}^\ell_{\mathrm{s}}(Y)$ the subspace of symmetric-valued functions in $\mathbf{P}^\ell(Y)$.

For all $T \in \mathcal{T}_h$, let $\boldsymbol{x}_T \in T$ be such that T contains a ball centered at $\boldsymbol{x}_T$ of radius ρh_T, where ρ is the mesh regularity parameter in [20, Assumption 7.6]. For any integer $\ell \geq 0$, we define the following relevant subspaces of $\boldsymbol{\mathcal{P}}^\ell(T)$:

$$\boldsymbol{\mathcal{R}}^\ell(T) := \mathbf{rot}\,\mathcal{P}^{\ell+1}(T), \qquad \boldsymbol{\mathcal{R}}^{\mathrm{c},\ell}(T) := (\boldsymbol{x} - \boldsymbol{x}_T)\mathcal{P}^{\ell-1}(T), \tag{5}$$

where, for a vector $\boldsymbol{y} \in \mathbb{R}^2$, $\boldsymbol{y}^\perp$ denotes the vector obtained rotating $\boldsymbol{y}$ by $-\frac{\pi}{2}$. We have

$$\boldsymbol{\mathcal{P}}^\ell(T) = \boldsymbol{\mathcal{R}}^\ell(T) \oplus \boldsymbol{\mathcal{R}}^{\mathrm{c},\ell}(T). \tag{6}$$

Notice that the direct sums in the above expression are not L^2-orthogonal in general. The L^2-orthogonal projectors on the spaces (5) are, with obvious notation, $\boldsymbol{\pi}^\ell_{\boldsymbol{\mathcal{R}},T}$, and $\boldsymbol{\pi}^{\mathrm{c},\ell}_{\boldsymbol{\mathcal{R}},T}$.

3 DDR scheme

The scheme for (2) is designed using spaces of unknowns from the DDR method [19] together with an enrichment inspired by HHO methods [20].

3.1 Spaces and interpolators

Let a polynomial degree $k \geq 0$ be fixed and set

$$\begin{aligned}
\underline{\boldsymbol{\Theta}}_h^k &:= \Big\{\underline{\boldsymbol{\eta}}_h = \big((\boldsymbol{\eta}_{\mathcal{R},T}, \boldsymbol{\eta}^{\mathrm{c}}_{\mathcal{R},T})_{T\in\mathcal{T}_h}, (\boldsymbol{\eta}_E)_{E\in\mathcal{E}_h}\big) \,:\, (\boldsymbol{\eta}_{\mathcal{R},T}, \boldsymbol{\eta}^{\mathrm{c}}_{\mathcal{R},T}) \in \boldsymbol{\mathcal{R}}^{k-1}(T) \times \boldsymbol{\mathcal{R}}^{\mathrm{c},k}(T) \text{ for all } T \in \mathcal{T}_h, \\
&\qquad\qquad \text{and } \boldsymbol{\eta}_E \in \boldsymbol{\mathcal{P}}^k(E) \text{ for all } E \in \mathcal{E}_h\Big\}, \\
\underline{U}_h^k &:= \Big\{\underline{v}_h = \big((v_T)_{T\in\mathcal{T}_h}, v_{\mathcal{E}_h}\big) \,:\, v_T \in \mathcal{P}^{k-1}(T) \text{ for all } T \in \mathcal{T}_h \text{ and } v_{\mathcal{E}_h} \in \mathcal{P}^{k+1}_{\mathrm{c}}(\mathcal{E}_h)\Big\},
\end{aligned}$$

where $\mathcal{P}^{k+1}_{\mathrm{c}}(\mathcal{E}_h)$ is spanned by the functions over the mesh edge skeleton whose restriction to each edge $E \in \mathcal{E}_h$ is a polynomial of total degree $\leq k+1$ and that are continuous at the edges endpoints. The space $\underline{\boldsymbol{\Theta}}_h^k$ is an enrichment of the two-dimensional DDR space $\underline{\boldsymbol{X}}^k_{\mathbf{curl},h}$ with edge unknowns representing a full vector-valued field as opposed to its tangent component only; the space $\underline{U}_h^k$ coincides with the two-dimensional DDR space $\underline{\boldsymbol{X}}^k_{\mathbf{grad},h}$.

Smooth functions are interpolated as follows: For all $\boldsymbol{\eta} \in H^1(\Omega)^2$

$$\underline{\boldsymbol{I}}^k_{\boldsymbol{\Theta},h}\boldsymbol{\eta} \coloneqq \big((\boldsymbol{\pi}^{k-1}_{\mathcal{R},T}\boldsymbol{\eta}_{|T}, \boldsymbol{\pi}^{\mathrm{c},k}_{\mathcal{R},T}\boldsymbol{\eta}_{|T})_{T\in\mathcal{T}_h}, (\boldsymbol{\pi}^k_{\mathcal{P},E}\boldsymbol{\eta}_{|E})_{E\in\mathcal{E}_h}\big) \in \underline{\boldsymbol{\Theta}}^k_h, \tag{7}$$

while, for all $v \in C^0(\overline{\Omega})$,

$$\underline{I}^k_{U,h}v \coloneqq \big((\pi^{k-1}_{\mathcal{P},T}v_{|T})_{T\in\mathcal{T}_h}, v_{\mathcal{E}_h}\big) \in \underline{U}^k_h,$$
$$\text{with } \pi^{k-1}_{\mathcal{P},E}(v_{\mathcal{E}_h})_{|E} = \pi^{k-1}_{\mathcal{P},E}v_{|E} \text{ for all } E \in \mathcal{E}_h \text{ and } v_{\mathcal{E}_h}(\boldsymbol{x}_V) = v(\boldsymbol{x}_V) \text{ for all } V \in \mathcal{V}_h.$$

For all $T \in \mathcal{T}_h$, we denote by $\underline{\boldsymbol{\Theta}}^k_T$ and $\underline{U}^k_T$, respectively, the restrictions of $\underline{\boldsymbol{\Theta}}^k_h$ and $\underline{U}^k_h$ to T, collecting the polynomial components that lie inside T and on its boundary. A similar convention is adopted for the elements of these spaces and for the interpolators.

3.2 Discrete differential operators and potentials

We introduce discrete versions of the differential operators and of the rotation field reconstructed from the unknowns in the discrete spaces.

3.2.1 Discrete gradient and transverse displacement reconstruction on $\underline{U}^k_T$

We follow here standard constructions from the DDR method. For all $T \in \mathcal{T}_h$, the polynomial transverse displacement gradient $\boldsymbol{G}^k_T : \underline{U}^k_T \to \boldsymbol{\mathcal{P}}^k(T)$ is such that, for all $\underline{v}_T \in \underline{U}^k_T$,

$$\int_T \boldsymbol{G}^k_T\underline{v}_T \cdot \boldsymbol{\eta} = -\int_T v_T \operatorname{div}\boldsymbol{\eta} + \sum_{E\in\mathcal{E}_T}\omega_{TE}\int_E v_{\mathcal{E}_T}(\boldsymbol{\eta}\cdot\boldsymbol{n}_E) \qquad \forall\boldsymbol{\eta} \in \boldsymbol{\mathcal{P}}^k(T). \tag{8}$$

We additionally define the transverse displacement reconstruction $P^{k+1}_{U,T} : \underline{U}^k_T \to \mathcal{P}^{k+1}(T)$ such that, for all $\underline{v}_T \in \underline{U}^k_T$,

$$\int_T P^{k+1}_{U,T}\underline{v}_T \operatorname{div}\boldsymbol{\eta} = -\int_T \boldsymbol{G}^k_T\underline{v}_T \cdot \boldsymbol{\eta} + \sum_{E\in\mathcal{E}_T}\omega_{TE}\int_E v_{\mathcal{E}_T}(\boldsymbol{\eta}\cdot\boldsymbol{n}_E) \qquad \forall\boldsymbol{\eta} \in \boldsymbol{\mathcal{R}}^{\mathrm{c},k+2}(T).$$

A global transverse displacement reconstruction is obtained setting, for all $\underline{v}_h \in \underline{U}^k_h$,

$$(P^{k+1}_{U,h}\underline{v}_h)_{|T} \coloneqq P^{k+1}_{U,T}\underline{v}_T \qquad \forall T \in \mathcal{T}_h.$$

Finally, we define a global discrete transverse displacement gradient $\underline{\boldsymbol{G}}^k_h : \underline{U}^k_h \to \underline{\boldsymbol{\Theta}}^k_h$ as follows: For all $\underline{v}_h \in \underline{U}^k_h$,

$$\underline{\boldsymbol{G}}^k_h\underline{v}_h \coloneqq \big((\boldsymbol{\pi}^{k-1}_{\mathcal{R},T}\boldsymbol{G}^k_T\underline{v}_T, \boldsymbol{\pi}^{\mathrm{c},k}_{\mathcal{R},T}\boldsymbol{G}^k_T\underline{v}_T)_{T\in\mathcal{T}_h}, ((v_{\mathcal{E}_h})'_{|E}\boldsymbol{t}_E)_{E\in\mathcal{E}_h}\big),$$

where the derivative along the edge is taken in the direction of $\boldsymbol{t}_E$.

To state the key commutation property used to prove the error estimates for the DDR scheme, we need to introduce a modified version of the interpolator on $\underline{\boldsymbol{\Theta}}^k_h$, which is adjusted to the account for the fact that, on the edges, the discrete gradient only encodes the tangential derivatives. The modified interpolator is $\underline{\boldsymbol{I}}^{\flat,k}_{\boldsymbol{\Theta},h} : H^1(\Omega)^2 \to \underline{\boldsymbol{\Theta}}^k_h$ such that, for all $\boldsymbol{\eta} \in H^1(\Omega)^2$,

$$\underline{\boldsymbol{I}}^{\flat,k}_{\boldsymbol{\Theta},h}\boldsymbol{\eta} \coloneqq \big((\boldsymbol{\pi}^{k-1}_{\mathcal{R},T}\boldsymbol{\eta}_{|T}, \boldsymbol{\pi}^{\mathrm{c},k}_{\mathcal{R},T}\boldsymbol{\eta}_{|T})_{T\in\mathcal{T}_h}, (\pi^k_{\mathcal{P},E}(\boldsymbol{\eta}_{|E}\cdot\boldsymbol{t}_E)\,\boldsymbol{t}_E)_{E\in\mathcal{E}_h}\big). \tag{9}$$

The commutation property is the following, obtained by considering only the face components in the 3D formula [19, Eq. (3.33)]:

$$\underline{\boldsymbol{G}}^k_h(\underline{I}^k_{U,h}v) = \underline{\boldsymbol{I}}^{\flat,k}_{\boldsymbol{\Theta},h}(\mathbf{grad}\, v) \qquad \forall v \in C^1(\overline{\Omega}). \tag{10}$$

3.2.2 Discrete scalar rotor and rotation reconstruction on $\underline{\boldsymbol{\Theta}}_T^k$

Let a mesh element $T \in \mathcal{T}_h$ be fixed. The local scalar rotor operator $R_T^k : \underline{\boldsymbol{\Theta}}_T^k \to \mathcal{P}^k(T)$ is such that, for all $\underline{\boldsymbol{\eta}}_T \in \underline{\boldsymbol{\Theta}}_T^k$,

$$\int_T R_T^k \underline{\boldsymbol{\eta}}_T q = \int_T \boldsymbol{\eta}_{\mathcal{R},T} \cdot \mathbf{rot}\, q - \sum_{E \in \mathcal{E}_T} \omega_{TE} \int_E (\boldsymbol{\eta}_E \cdot \boldsymbol{t}_E)\, q \qquad \forall q \in \mathcal{P}^k(T). \tag{11}$$

This operator enables the reconstruction of a discrete rotation $\boldsymbol{P}_{\boldsymbol{\Theta},T}^k : \underline{\boldsymbol{\Theta}}_T^k \to \boldsymbol{\mathcal{P}}^k(T)$ defined such that, for all $\underline{\boldsymbol{\eta}}_T \in \underline{\boldsymbol{\Theta}}_T^k$ and all $(\boldsymbol{\tau}, q) \in \boldsymbol{\mathcal{R}}^{\mathrm{c},k}(T) \times \mathcal{P}^{k+1}(T)$,

$$\int_T \boldsymbol{P}_{\boldsymbol{\Theta},T}^k \underline{\boldsymbol{\eta}}_T \cdot (\boldsymbol{\tau} + \mathbf{rot}\, q) = \int_T \boldsymbol{\eta}_{\mathcal{R},T}^{\mathrm{c}} \cdot \boldsymbol{\tau} + \int_T R_T^k \underline{\boldsymbol{\eta}}_T\, q + \sum_{E \in \mathcal{E}_T} \omega_{TE} \int_E (\boldsymbol{\eta}_E \cdot \boldsymbol{t}_E)\, q. \tag{12}$$

The scalar rotor and rotation reconstructions correspond to the face curl and tangential face potential of the DDR method [19, Eqs. (3.15) and (3.18)]. We note the following property [19, Proposition 15]: For all $\underline{\boldsymbol{\eta}}_T \in \underline{\boldsymbol{\Theta}}_T^k$,

$$\boldsymbol{\pi}_{\mathcal{R},T}^{k-1}(\boldsymbol{P}_{\boldsymbol{\Theta},T}^k \underline{\boldsymbol{\eta}}_T) = \boldsymbol{\eta}_{\mathcal{R},T} \quad \text{and} \quad \boldsymbol{\pi}_{\mathcal{R},T}^{\mathrm{c},k}(\boldsymbol{P}_{\boldsymbol{\Theta},T}^k \underline{\boldsymbol{\eta}}_T) = \boldsymbol{\eta}_{\mathcal{R},T}^{\mathrm{c}}. \tag{13}$$

In consequence, for all $\boldsymbol{\eta} \in H^1(T)^2$, we have $\boldsymbol{\pi}_{\mathcal{R},T}^{k-1}\left[\boldsymbol{P}_{\boldsymbol{\Theta},T}^k(\underline{\boldsymbol{I}}_{\boldsymbol{\Theta},T}^k \boldsymbol{\eta})\right] = \boldsymbol{\pi}_{\mathcal{R},T}^{k-1}\boldsymbol{\eta}$ and $\boldsymbol{\pi}_{\mathcal{R},T}^{\mathrm{c},k-1}\left[\boldsymbol{P}_{\boldsymbol{\Theta},T}^k(\underline{\boldsymbol{I}}_{\boldsymbol{\Theta},T}^k \boldsymbol{\eta})\right] = \boldsymbol{\pi}_{\mathcal{R},T}^{\mathrm{c},k-1}\boldsymbol{\eta}$ (where we have used $\boldsymbol{\mathcal{R}}^{\mathrm{c},k-1}(T) \subset \boldsymbol{\mathcal{R}}^{\mathrm{c},k}(T)$, see (5), to write $\boldsymbol{\pi}_{\mathcal{R},T}^{\mathrm{c},k-1} = \boldsymbol{\pi}_{\mathcal{R},T}^{\mathrm{c},k-1}\boldsymbol{\pi}_{\mathcal{R},T}^{\mathrm{c},k}$). Combining these relations with (6) written for $\ell = k-1$ and [19, Lemma 4], we get

$$\boldsymbol{\pi}_{\mathcal{P},T}^{k-1}\left[\boldsymbol{P}_{\boldsymbol{\Theta},T}^k(\underline{\boldsymbol{I}}_{\boldsymbol{\Theta},T}^k \boldsymbol{\eta})\right] = \boldsymbol{\pi}_{\mathcal{P},T}^{k-1}\boldsymbol{\eta} \qquad \forall \boldsymbol{\eta} \in H^1(T)^2. \tag{14}$$

3.2.3 Discrete symmetric gradient, divergence and stabilisation on $\underline{\boldsymbol{\Theta}}_T^k$

The discretisation of the bilinear form (3) requires to define a discrete symmetric gradient (and divergence) on the discrete space of rotations. Since vectors in this space have polynomial components inside the elements and on the edges, a natural approach to define such discrete differential operators comes from the Hybrid High-Order (HHO) machinery [20]. In what follows, we let a mesh element $T \in \mathcal{T}_h$ be fixed.

Gradients and divergence. Let us define the local (vector-valued) HHO space, extension of $\underline{\boldsymbol{\Theta}}_T^k$ in which the element component is taken in the full polynomial space:

$$\underline{\boldsymbol{\Theta}}_{\mathrm{HHO},T}^k = \left\{\underline{\boldsymbol{w}}_T = (\boldsymbol{w}_T, (\boldsymbol{w}_E)_{E \in \mathcal{E}_T}) \,:\, \boldsymbol{w}_T \in \boldsymbol{\mathcal{P}}^k(T), \quad \boldsymbol{w}_E \in \boldsymbol{\mathcal{P}}^k(E) \quad \forall E \in \mathcal{E}_T\right\}. \tag{15}$$

The discrete rotation enables the definition of the following embedding $\underline{\boldsymbol{\mathfrak{I}}}_{\mathrm{HHO},T}^k : \underline{\boldsymbol{\Theta}}_T^k \to \underline{\boldsymbol{\Theta}}_{\mathrm{HHO},T}^k$:

$$\underline{\boldsymbol{\mathfrak{I}}}_{\mathrm{HHO},T}^k \underline{\boldsymbol{\eta}}_T := (\boldsymbol{P}_{\boldsymbol{\Theta},T}^k \underline{\boldsymbol{\eta}}_T, (\boldsymbol{\eta}_E)_{E \in \mathcal{E}_T}) \qquad \forall \underline{\boldsymbol{\eta}}_T \in \underline{\boldsymbol{\Theta}}_T^k. \tag{16}$$

Owing to (13), $\underline{\boldsymbol{\mathfrak{I}}}_{\mathrm{HHO},T}^k$ is indeed a one-to-one mapping.

Using HHO techniques (see in particular [20, Section 7.2.5]) on $\underline{\boldsymbol{\mathfrak{I}}}_{\mathrm{HHO},T}^k \underline{\boldsymbol{\eta}}_T$, we can then design the local discrete gradients (standard and symmetric) and divergence of a discrete rotation $\underline{\boldsymbol{\eta}}_T \in \underline{\boldsymbol{\Theta}}_T^k$. Specifically, this leads to defining the rotation gradient $\mathbf{G}_T^k : \underline{\boldsymbol{\Theta}}_T^k \to \mathbf{P}^k(T)$ such that, for all $\underline{\boldsymbol{\eta}}_T \in \underline{\boldsymbol{\Theta}}_T^k$,

$$\int_T \mathbf{G}_T^k \underline{\boldsymbol{\eta}}_T : \mathbf{t} = -\int_T \boldsymbol{P}_{\boldsymbol{\Theta},T}^k \underline{\boldsymbol{\eta}}_T \cdot (\mathbf{div}\, \mathbf{t}) + \sum_{E \in \mathcal{E}_T} \omega_{TE} \int_E \boldsymbol{\eta}_E \cdot (\mathbf{t}\boldsymbol{n}_E) \qquad \forall \mathbf{t} \in \mathbf{P}^k(T). \tag{17}$$

The local symmetric gradient $\mathsf{G}^k_{\mathrm{s},T} : \underline{\boldsymbol{\Theta}}^k_T \to \mathsf{P}^k_{\mathrm{s}}(T)$ and divergence $D^k_T : \underline{\boldsymbol{\Theta}}^k_T \to \mathcal{P}^k(T)$ are obtained setting, for all $\underline{\boldsymbol{\eta}}_T \in \underline{\boldsymbol{\Theta}}^k_T$,

$$\mathsf{G}^k_{\mathrm{s},T}\underline{\boldsymbol{\eta}}_T := \frac{1}{2}\left[\mathsf{G}^k_T\underline{\boldsymbol{\eta}}_T + (\mathsf{G}^k_T\underline{\boldsymbol{\eta}}_T)^{\mathsf{T}}\right], \qquad D^k_T\underline{\boldsymbol{\eta}}_T := \mathrm{tr}(\mathsf{G}^k_T\underline{\boldsymbol{\eta}}_T).$$

In (17), since $\mathbf{div}\,\mathbf{t} \in \mathcal{P}^{k-1}(T)$ we can replace $\boldsymbol{P}^k_{\boldsymbol{\Theta},T}\underline{\boldsymbol{\eta}}_T$ with $\boldsymbol{\pi}^{k-1}_{\mathcal{P},T}(\boldsymbol{P}^k_{\boldsymbol{\Theta},T}\underline{\boldsymbol{\eta}}_T)$ and thus, using (14) and following the techniques of [20, Section 7.2.5], we obtain the commutation formula $\mathsf{G}^k_T(\underline{\boldsymbol{I}}^k_{\boldsymbol{\Theta},T}\boldsymbol{\eta}) = \boldsymbol{\pi}^k_{\mathcal{P},T}(\mathbf{grad}\,\boldsymbol{\eta})$ for all $\boldsymbol{\eta} \in H^1(T)^2$; this shows that G^k_T (hence also $\mathsf{G}^k_{\mathrm{s},T}$ and D^k_T) has optimal approximation properties.

Stabilisation. As usual in numerical methods for polytopal meshes, the discrete counterpart of a bilinear form such as (3) involves a consistent component (here, based on $\mathsf{G}^k_{\mathrm{s},T}$), and a stabilisation term. In HHO methods, the local stabilisation bilinear forms are defined through the introduction of a higher-order reconstruction. For elasticity problems involving the discrete symmetric gradient, and accounting for the embedding (16), this leads to defining $\boldsymbol{p}^{k+1}_T : \underline{\boldsymbol{\Theta}}_T \to \mathcal{P}^{k+1}(T)$ by: For all $\underline{\boldsymbol{\eta}}_T \in \underline{\boldsymbol{\Theta}}_T$ and all $\boldsymbol{w} \in \mathcal{P}^{k+1}(T)$,

$$\int_T \mathbf{grad}_{\mathrm{s}}\,\boldsymbol{p}^{k+1}_T\underline{\boldsymbol{\eta}}_T : \mathbf{grad}_{\mathrm{s}}\,\boldsymbol{w} = -\int_T \boldsymbol{P}^k_{\boldsymbol{\Theta},T}\underline{\boldsymbol{\eta}}_T \cdot \mathbf{div}(\mathbf{grad}_{\mathrm{s}}\,\boldsymbol{w}) + \sum_{E\in\mathcal{E}_T}\int_E \boldsymbol{\eta}_E \cdot (\mathbf{grad}_{\mathrm{s}}\,\boldsymbol{w}\,\boldsymbol{n}_{TE}), \tag{18a}$$

$$\int_T \mathbf{grad}_{\mathrm{ss}}\,\boldsymbol{p}^{k+1}_T\underline{\boldsymbol{\eta}}_T = \frac{1}{2}\sum_{E\in\mathcal{E}_T}\int_E (\boldsymbol{\eta}_E \otimes \boldsymbol{n}_{TE} - \boldsymbol{n}_{TE} \otimes \boldsymbol{\eta}_E)\,, \text{ and} \tag{18b}$$

$$\int_T \boldsymbol{p}^{k+1}_T\underline{\boldsymbol{\eta}}_T = \int_T \boldsymbol{P}^k_{\boldsymbol{\Theta},T}\underline{\boldsymbol{\eta}}_T \quad \text{if } k \geq 1, \qquad \int_{\partial T} \boldsymbol{p}^{k+1}_T\underline{\boldsymbol{\eta}}_T = \sum_{E\in\mathcal{E}_T}\int_E \boldsymbol{\eta}_E \quad \text{if } k = 0. \tag{18c}$$

In a similar way as for G^k_T above, in (18a) the term $\boldsymbol{P}^k_{\boldsymbol{\Theta},T}\underline{\boldsymbol{\eta}}_T$ can be replaced with $\boldsymbol{\pi}^{k-1}_{\mathcal{P},T}(\boldsymbol{P}^k_{\boldsymbol{\Theta},T}\underline{\boldsymbol{\eta}}_T)$ (because $\mathbf{div}(\mathbf{grad}_{\mathrm{s}}\,\boldsymbol{w}) \in \mathcal{P}^{k-1}(T)$). Hence, using (14) and the techniques of [20, Section 7.2.5] we see that, for $k \geq 1$,

$$\boldsymbol{p}^{k+1}_T(\underline{\boldsymbol{I}}^k_{\boldsymbol{\Theta},T}\boldsymbol{\eta}) = \boldsymbol{\pi}^{k+1}_{\boldsymbol{\varepsilon},T}\boldsymbol{\eta} \qquad \forall \boldsymbol{\eta} \in H^1(T)^2, \tag{19}$$

where $\boldsymbol{\pi}^{k+1}_{\boldsymbol{\varepsilon},T} : H^1(T)^2 \to \mathcal{P}^{k+1}(T)$ is the strain projector of degree $k+1$, see [20, Section 7.2.2]. If $k = 0$, the relation (19) is still verified with a modified version of the strain projector (still denoted by $\boldsymbol{\pi}^1_{\boldsymbol{\varepsilon},T}$), inspired by the modified elliptic projector of [20, Section 5.1.2], whose closure equation involves the average over ∂T instead of the average over T; this modified strain projector has the same approximation properties as the standard strain projector.

The local stabilisation is then defined by:

$$\mathrm{s}_T(\underline{\boldsymbol{\tau}}_T, \underline{\boldsymbol{\eta}}_T) = \sum_{E\in\mathcal{E}_T} h_T^{-1}\int_E (\boldsymbol{\delta}^k_{TE} - \boldsymbol{\delta}^k_T)\underline{\boldsymbol{\tau}}_T \cdot (\boldsymbol{\delta}^k_{TE} - \boldsymbol{\delta}^k_T)\underline{\boldsymbol{\eta}}_T \quad \forall \underline{\boldsymbol{\tau}}_T, \underline{\boldsymbol{\eta}}_T \in \underline{\boldsymbol{\Theta}}^k_T,$$

where the difference operators are such that, for all $\underline{\boldsymbol{\eta}}_T \in \underline{\boldsymbol{\Theta}}^k_T$ and $E \in \mathcal{E}_T$,

$$\boldsymbol{\delta}^k_T\underline{\boldsymbol{\eta}}_T := \boldsymbol{P}^k_{\boldsymbol{\Theta},T}\left[\underline{\boldsymbol{I}}^k_{\boldsymbol{\Theta},T}(\boldsymbol{p}^{k+1}_T\underline{\boldsymbol{\eta}}_T - \boldsymbol{P}^k_{\boldsymbol{\Theta},T}\underline{\boldsymbol{\eta}}_T)\right], \quad \boldsymbol{\delta}^k_{TE}\underline{\boldsymbol{\eta}}_T := \boldsymbol{\pi}^k_{\mathcal{P},E}(\boldsymbol{p}^{k+1}_T\underline{\boldsymbol{\eta}}_T - \boldsymbol{\eta}_E). \tag{20}$$

Observing that $\boldsymbol{P}^k_{\boldsymbol{\Theta},T}\underline{\boldsymbol{I}}^k_{\boldsymbol{\Theta},T} : H^1(T)^2 \to \mathcal{P}^k(T)$ is a projector (see [19, Eq. (3.21)]) and using (19), it can be checked that $\boldsymbol{\delta}^k_T(\underline{\boldsymbol{I}}^k_{\boldsymbol{\Theta},T}\boldsymbol{\eta}) = \mathbf{0}$ and $\boldsymbol{\delta}^k_{TE}(\underline{\boldsymbol{I}}^k_{\boldsymbol{\Theta},T}\boldsymbol{\eta}) = \mathbf{0}$ for all $E \in \mathcal{E}_T$, whenever $\boldsymbol{\eta} \in \mathcal{P}^{k+1}(T)$. As a consequence, we have the following polynomial consistency property for s_T:

$$\mathrm{s}_T(\underline{\boldsymbol{I}}^k_{\boldsymbol{\Theta},T}\boldsymbol{\eta}, \underline{\boldsymbol{\xi}}_T) = 0 \qquad \forall (\boldsymbol{\eta}, \underline{\boldsymbol{\xi}}_T) \in \mathcal{P}^{k+1}(T) \times \underline{\boldsymbol{\Theta}}^k_T. \tag{21}$$

Remark 1 (Original HHO stabilisation). In the original HHO stabilisation, the L^2-projector $\boldsymbol{\pi}^k_{\mathcal{P},T}$ is used instead of $\boldsymbol{P}^k_{\boldsymbol{\Theta},T}\underline{\boldsymbol{I}}^k_{\boldsymbol{\Theta},T}$ in the expression of $\boldsymbol{\delta}^k_T$; see (20). The reason for using $\boldsymbol{P}^k_{\boldsymbol{\Theta},T}\underline{\boldsymbol{I}}^k_{\boldsymbol{\Theta},T}$ here lies in the need to satisfy, for the interpolator $\underline{\boldsymbol{I}}^k_{\boldsymbol{\Theta},T}$ on $\underline{\boldsymbol{\Theta}}^k_T$, the polynomial consistency (21). Note also that, in s_T, the scaling factor h_T^{-1} has been preferred over the original HHO scaling factor h_E^{-1}, as it is proved in [23] to lead to a more robust discretisation in presence of small edges.

Using the L^2-boundedness of $\boldsymbol{P}^k_{\boldsymbol{\Theta},T}\underline{\boldsymbol{I}}^k_{\boldsymbol{\Theta},T}$ (stemming from the two-dimensional versions of [19, Proposition 27 and Lemma 28]), the commutation property (19), and the polynomial consistency (21), it is easy to reproduce, with our definitions of $\mathbf{G}^k_{\mathrm{s},T}$, $\boldsymbol{p}^{k+1}_T$ and s_T, the standard HHO analysis of [20, Section 7] and to obtain corresponding boundedness and consistency results (translated through $\underline{\boldsymbol{\mathfrak{I}}}^k_{\mathrm{HHO},T}$).

Global operators. Global symmetric gradient, divergence, and higher-order reconstruction operators are obtained setting, for all $\underline{\boldsymbol{\eta}}_h \in \underline{\boldsymbol{\Theta}}^k_h$,

$$(\mathbf{G}^k_{\mathrm{s},h}\underline{\boldsymbol{\eta}}_h)_{|T} := \mathbf{G}^k_{\mathrm{s},T}\underline{\boldsymbol{\eta}}_T,\ (D^k_h\underline{\boldsymbol{\eta}}_h)_{|T} := D^k_T\underline{\boldsymbol{\eta}}_T, \text{ and } (\boldsymbol{p}^{k+1}_h\underline{\boldsymbol{\eta}}_h)_{|T} = \boldsymbol{p}^{k+1}_T\underline{\boldsymbol{\eta}}_T \text{ for all } T \in \mathcal{T}_h.$$

Likewise, denoting by $\underline{\boldsymbol{\Theta}}^k_{\mathrm{HHO},h}$ the global HHO space obtained patching together the local spaces (15) by enforcing the single-valuedness of the edge components, we define the global embedding $\underline{\boldsymbol{\mathfrak{I}}}^k_{\mathrm{HHO},h} : \underline{\boldsymbol{\Theta}}^k_h \to \underline{\boldsymbol{\Theta}}^k_{\mathrm{HHO},h}$ by setting, for all $\underline{\boldsymbol{\eta}}_h \in \underline{\boldsymbol{\Theta}}^k_h$, $(\underline{\boldsymbol{\mathfrak{I}}}^k_{\mathrm{HHO},h}\underline{\boldsymbol{\eta}}_h)_{|T} := \underline{\boldsymbol{\mathfrak{I}}}^k_{\mathrm{HHO},T}\underline{\boldsymbol{\eta}}_T$ for all $T \in \mathcal{T}_h$. We also let $\mathrm{s}_h : \underline{\boldsymbol{\Theta}}^k_h \times \underline{\boldsymbol{\Theta}}^k_h \to \mathbb{R}$ be the global stabilisation bilinear form such that

$$\mathrm{s}_h(\underline{\boldsymbol{\tau}}_h, \underline{\boldsymbol{\eta}}_h) := \sum_{T\in\mathcal{T}_h} \mathrm{s}_T(\underline{\boldsymbol{\tau}}_T, \underline{\boldsymbol{\eta}}_T) \qquad \forall (\underline{\boldsymbol{\tau}}_h, \underline{\boldsymbol{\eta}}_h) \in \underline{\boldsymbol{\Theta}}^k_h \times \underline{\boldsymbol{\Theta}}^k_h.$$

3.3 Discrete forms

Based on the reconstructions introduced in the previous section, we define the discrete counterparts of the forms that appear in the weak formulation (2). Specifically, we let the bilinear form $\mathrm{A}_h : \left[\underline{\boldsymbol{\Theta}}^k_h \times \underline{U}^k_h\right]^2 \to \mathbb{R}$ and the linear form $\ell_h : \underline{U}^k_h \to \mathbb{R}$ be such that, for all $(\underline{\boldsymbol{\tau}}_h, \underline{w}_h), (\underline{\boldsymbol{\eta}}_h, \underline{v}_h) \in \underline{\boldsymbol{\Theta}}^k_h \times \underline{U}^k_h$,

$$\mathrm{A}_h((\underline{\boldsymbol{\tau}}_h, \underline{w}_h), (\underline{\boldsymbol{\eta}}_h, \underline{v}_h)) := \mathrm{a}_h(\underline{\boldsymbol{\tau}}_h, \underline{\boldsymbol{\eta}}_h) + \mathrm{b}_h((\underline{\boldsymbol{\tau}}_h, \underline{w}_h), (\underline{\boldsymbol{\eta}}_h, \underline{v}_h)), \qquad \ell_h(\underline{v}_h) := \int_\Omega f\, P^{k+1}_{U,h}\underline{v}_h, \tag{22}$$

where the bilinear forms $\mathrm{a}_h : \underline{\boldsymbol{\Theta}}^k_h \times \underline{\boldsymbol{\Theta}}^k_h \to \mathbb{R}$ and $\mathrm{b}_h : \left[\underline{\boldsymbol{\Theta}}^k_h \times \underline{U}^k_h\right]^2 \to \mathbb{R}$ are such that

$$\begin{gathered}\mathrm{a}_h(\underline{\boldsymbol{\tau}}_h, \underline{\boldsymbol{\eta}}_h) := \beta_0\left(\int_\Omega \mathbf{G}^k_{\mathrm{s},h}\underline{\boldsymbol{\tau}}_h : \mathbf{G}^k_{\mathrm{s},h}\underline{\boldsymbol{\eta}}_h + \mathrm{s}_h(\underline{\boldsymbol{\tau}}_h, \underline{\boldsymbol{\eta}}_h) + \mathrm{j}_h(\underline{\boldsymbol{\tau}}_h, \underline{\boldsymbol{\eta}}_h)\right) + \beta_1\int_\Omega D^k_h\underline{\boldsymbol{\tau}}_h\, D^k_h\underline{\boldsymbol{\eta}}_h,\\ \mathrm{b}_h((\underline{\boldsymbol{\tau}}_h, \underline{w}_h), (\underline{\boldsymbol{\eta}}_h, \underline{v}_h)) := \frac{\kappa}{t^2}(\underline{\boldsymbol{\tau}}_h - \underline{\boldsymbol{G}}^k_h\underline{w}_h, \underline{\boldsymbol{\eta}}_h - \underline{\boldsymbol{G}}^k_h\underline{v}_h)_{\boldsymbol{\Theta},h}.\end{gathered} \tag{23}$$

Here, j_h is an additional stabilisation term appearing only in the case $k = 0$ and which penalises the jumps of higher-order reconstructions between elements:

$$\mathrm{j}_h(\underline{\boldsymbol{\tau}}_h, \underline{\boldsymbol{\eta}}_h) := \begin{cases} 0 & \text{if } k \geq 1,\\ \displaystyle\sum_{E\in\mathcal{E}_h} h_E^{-1}\int_E [\boldsymbol{p}^1_h\underline{\boldsymbol{\tau}}_h]_E[\boldsymbol{p}^1_h\underline{\boldsymbol{\eta}}_h]_E & \text{if } k = 0,\end{cases}$$

where, for any internal edge $E \in \mathcal{E}^{\mathrm{i}}_h$, if T_1, T_2 are the two elements (in an arbitrary but fixed order) on each side of E, we set $[\boldsymbol{p}^1_h\underline{\boldsymbol{\tau}}_h]_E := (\boldsymbol{p}^1_{T_1}\underline{\boldsymbol{\tau}}_{T_1})_{|E} - (\boldsymbol{p}^1_{T_2}\underline{\boldsymbol{\tau}}_{T_2})_{|E}$ while, for any boundary edge $E \in \mathcal{E}^{\mathrm{b}}_h \cap \mathcal{E}_T$

for $T \in \mathcal{T}_h$, $[\boldsymbol{p}_h^1 \underline{\boldsymbol{\tau}}_h]_E := (\boldsymbol{p}_T^1 \underline{\boldsymbol{\tau}}_T)_{|E}$. We also introduced in (23) the DDR L^2-product $(\cdot,\cdot)_{\boldsymbol{\Theta},h}$ on $\underline{\boldsymbol{\Theta}}_h^k$ assembled from the following local contributions: For all $\underline{\boldsymbol{\tau}}_T, \underline{\boldsymbol{\eta}}_T \in \underline{\boldsymbol{\Theta}}_T^k$,

$$
\begin{aligned}
(\underline{\boldsymbol{\tau}}_T, \underline{\boldsymbol{\eta}}_T)_{\boldsymbol{\Theta},T} &:= \int_T \boldsymbol{P}_{\boldsymbol{\Theta},T}^k \underline{\boldsymbol{\tau}}_T \cdot \boldsymbol{P}_{\boldsymbol{\Theta},T}^k \underline{\boldsymbol{\eta}}_T + \mathrm{S}_{\boldsymbol{\Theta},T}(\underline{\boldsymbol{\tau}}_T, \underline{\boldsymbol{\eta}}_T) \\
\text{with } \mathrm{S}_{\boldsymbol{\Theta},T}(\underline{\boldsymbol{\tau}}_T, \underline{\boldsymbol{\eta}}_T) &:= \sum_{E \in \mathcal{E}_T} h_E \int_E (\boldsymbol{P}_{\boldsymbol{\Theta},T}^k \underline{\boldsymbol{\tau}}_T - \boldsymbol{\tau}_E) \cdot \boldsymbol{t}_E \, (\boldsymbol{P}_{\boldsymbol{\Theta},T}^k \underline{\boldsymbol{\eta}}_T - \boldsymbol{\eta}_E) \cdot \boldsymbol{t}_E.
\end{aligned}
\tag{24}
$$

Remark 2 (Normal components of edge polynomials). A simple inspection of (11), (12) and (24) shows that the normal components of edge unknowns do not enter the definition of $(\cdot,\cdot)_{\boldsymbol{\Theta},h}$.

3.4 Discrete problem

Define the following subspaces of $\underline{\boldsymbol{\Theta}}_h^k$ and $\underline{U}_h^k$ incorporating the clamped boundary condition:

$$
\underline{\boldsymbol{\Theta}}_{h,0}^k := \left\{ \underline{\boldsymbol{\eta}}_h \in \underline{\boldsymbol{\Theta}}_h^k \,:\, \boldsymbol{\eta}_E = \boldsymbol{0} \text{ for all } E \in \mathcal{E}_h^{\mathrm{b}} \right\}, \qquad \underline{U}_{h,0}^k := \left\{ \underline{v}_h \in \underline{U}_h^k \,:\, (v_{\mathcal{E}_h})_{|\partial\Omega} = 0 \right\}.
$$

The discrete problem reads: Find $(\underline{\boldsymbol{\theta}}_h, \underline{u}_h) \in \underline{\boldsymbol{\Theta}}_{h,0}^k \times \underline{U}_{h,0}^k$ such that

$$
\mathrm{A}_h((\underline{\boldsymbol{\theta}}_h, \underline{u}_h), (\underline{\boldsymbol{\eta}}_h, \underline{v}_h)) = \ell_h(\underline{v}_h) \qquad \forall (\underline{\boldsymbol{\eta}}_h, \underline{v}_h) \in \underline{\boldsymbol{\Theta}}_{h,0}^k \times \underline{U}_{h,0}^k. \tag{25}
$$

4 Analysis

Let

$$
\mu := \min(\kappa, \beta_0). \tag{26}
$$

Throughout the rest of the paper, we use $a \lesssim b$ as a shorthand notation for the inequality $a \le Cb$ with multiplicative constant C that possibly depends on Ω, the mesh regularity, and on the polynomial degree, but not on β_0, β_1, κ, μ, t, or h and, for local inequalities, on the mesh element or edge.

4.1 Discrete norm and stability

We define the discrete seminorm on $\underline{\boldsymbol{\Theta}}_h^k \times \underline{U}_h^k$ such that, for all $(\underline{\boldsymbol{\eta}}_h, \underline{v}_h) \in \underline{\boldsymbol{\Theta}}_h^k \times \underline{U}_h^k$,

$$
\begin{aligned}
\|(\underline{\boldsymbol{\eta}}_h, \underline{v}_h)\|_{\boldsymbol{\Theta}\times U,h} := \Bigg[\beta_0 \left(\|\mathbf{G}_{\mathrm{s},h}^k \underline{\boldsymbol{\eta}}_h\|_{L^2(\Omega)^{2\times 2}}^2 + |\underline{\boldsymbol{\eta}}_h|_{\mathrm{s,j},h}^2 \right) + \beta_1 \|D_h^k \underline{\boldsymbol{\eta}}_h\|_{L^2(\Omega)}^2 \\
+ \frac{\kappa}{t^2} \|\underline{\boldsymbol{\eta}}_h - \underline{\boldsymbol{G}}_h^k \underline{v}_h\|_{\boldsymbol{\Theta},h}^2 + \mu \left(\|\underline{\boldsymbol{\eta}}_h\|_{\boldsymbol{\Theta},h}^2 + \|\underline{\boldsymbol{G}}_h^k \underline{v}_h\|_{\boldsymbol{\Theta},h}^2 \right) \Bigg]^{\frac{1}{2}},
\end{aligned}
\tag{27}
$$

where $\|\cdot\|_{\boldsymbol{\Theta},h}$ and $|\cdot|_{\mathrm{s,j},h}$ denote the seminorms respectively induced by $(\cdot,\cdot)_{\boldsymbol{\Theta},h}$ and $\mathrm{s}_h + \mathrm{j}_h$ on $\underline{\boldsymbol{\Theta}}_h^k$. Using, respectively, the discrete Korn and Korn–Poincaré inequalities [20, Lemma 7.24 and Eq. (7.73)] (see also [20, Lemma 7.42] in the case $k = 0$) and the fact that $h_E \le 1$ for the terms composing the norm in the left-hand side (see (24) for the corresponding local contribution), we readily obtain

$$
\|\underline{\boldsymbol{\eta}}_h\|_{\boldsymbol{\Theta},h} \lesssim \left(\|\mathbf{G}_{\mathrm{s},h}^k \underline{\boldsymbol{\eta}}_h\|_{L^2(\Omega)^{2\times 2}}^2 + |\underline{\boldsymbol{\eta}}_h|_{\mathrm{s,j},h}^2 \right)^{\frac{1}{2}} \qquad \forall \underline{\boldsymbol{\eta}}_h \in \underline{\boldsymbol{\Theta}}_{h,0}^k. \tag{28}
$$

Together with the Poincaré inequality for $\underline{\boldsymbol{G}}_h^k$ in $\underline{U}_{h,0}^k$, whose proof can be obtained using arguments similar to [19, Theorem 31] (leveraging the Poincaré inequality with zero boundary condition stated in [20, Lemma 2.15]), (28) proves that the energy seminorm $\|\cdot\|_{\boldsymbol{\Theta}\times U,h}$ is actually a norm on $\underline{\boldsymbol{\Theta}}_{h,0}^k \times \underline{U}_{h,0}^k$. We can now establish the coercivity of A_h with respect to this norm.

Lemma 3 (Coercivity)**.** *For all* $(\underline{\boldsymbol{\eta}}_h, \underline{v}_h) \in \underline{\boldsymbol{\Theta}}_{h,0}^k \times \underline{U}_{h,0}^k$*, it holds*

$$\|(\underline{\boldsymbol{\eta}}_h, \underline{v}_h)\|_{\boldsymbol{\Theta}\times U,h}^2 \lesssim \mathrm{A}_h((\underline{\boldsymbol{\eta}}_h, \underline{v}_h), (\underline{\boldsymbol{\eta}}_h, \underline{v}_h)). \tag{29}$$

Proof. By the definitions (22) of A_h and (23) of a_h and b_h, we have

$$\beta_0 \left(\|\mathbf{G}_{\mathrm{s},h}^k \underline{\boldsymbol{\eta}}_h\|_{L^2(\Omega)^{2\times 2}}^2 + |\underline{\boldsymbol{\eta}}_h|_{\mathrm{s,j},h}^2 \right) + \beta_1 \|D_h^k \underline{\boldsymbol{\eta}}_h\|_{L^2(\Omega)}^2 + \frac{\kappa}{t^2} \|\underline{\boldsymbol{\eta}}_h - \underline{\boldsymbol{G}}_h^k \underline{v}_h\|_{\boldsymbol{\Theta},h}^2 = \mathrm{A}_h((\underline{\boldsymbol{\tau}}_h, \underline{v}_h), (\underline{\boldsymbol{\tau}}_h, \underline{v}_h)). \tag{30}$$

We next write, using a triangle inequality,

$$\begin{aligned} \|\underline{\boldsymbol{G}}_h^k \underline{v}_h\|_{\boldsymbol{\Theta},h}^2 + \|\underline{\boldsymbol{\eta}}_h\|_{\boldsymbol{\Theta},h}^2 &\le 2\|\underline{\boldsymbol{\eta}}_h - \underline{\boldsymbol{G}}_h^k \underline{v}_h\|_{\boldsymbol{\Theta},h}^2 + 3\|\underline{\boldsymbol{\eta}}_h\|_{\boldsymbol{\Theta},h}^2 \\ &\le 2\kappa^{-1} \frac{\kappa}{t^2} \|\underline{\boldsymbol{\eta}}_h - \underline{\boldsymbol{G}}_h^k \underline{v}_h\|_{\boldsymbol{\Theta},h}^2 + 3\beta_0^{-1}\beta_0 \left(\|\mathbf{G}_{\mathrm{s},h}^k \underline{\boldsymbol{\eta}}_h\|_{L^2(\Omega)^{2\times 2}}^2 + |\underline{\boldsymbol{\eta}}_h|_{\mathrm{s,j},h}^2 \right) \\ &\lesssim \mu^{-1} \mathrm{A}_h((\underline{\boldsymbol{\tau}}_h, \underline{v}_h), (\underline{\boldsymbol{\tau}}_h, \underline{v}_h)), \end{aligned} \tag{31}$$

where we have used the fact that $t < 1$ along with the discrete Korn inequality (28) to pass to the second line and (30) together with the definition (26) of μ to conclude. The proof is completed by combining (30) and (31) with the definition of $\|\cdot\|_{\boldsymbol{\Theta}\times U,h}$. □

4.2 Error estimates

The regularity assumptions in the error estimates are expressed in terms of the broken Sobolev spaces

$$H^s(\mathcal{T}_h) := \left\{ v \in L^2(\Omega) \,:\, v_{|T} \in H^s(T) \text{ for all } T \in \mathcal{T}_h \right\}.$$

The first error estimate is for an arbitrary polynomial degree k.

Theorem 4 (Error estimate for arbitrary k)**.** *Denote by* $(\boldsymbol{\eta}, u) \in \boldsymbol{\Theta} \times U$ *and* $(\underline{\boldsymbol{\eta}}_h, \underline{u}_h) \in \underline{\boldsymbol{\Theta}}_{h,0}^k \times \underline{U}_{h,0}^k$ *the solutions to problems* (2) *and* (25)*, respectively. We assume the additional regularity* $u \in C^1(\overline{\Omega}) \cap H^{k+2}(\mathcal{T}_h)$ *for the displacement and* $\boldsymbol{\theta} \in H^1(\Omega)^2 \cap H^{k+2}(\mathcal{T}_h)^2$ *for the rotation. Then, it holds*

$$\|(\underline{\boldsymbol{\theta}}_h - \underline{\boldsymbol{I}}_{\boldsymbol{\Theta},h}^k \boldsymbol{\theta}, \underline{u}_h - \underline{I}_{U,h}^k u)\|_{\boldsymbol{\Theta}\times U,h} \lesssim h^{k+1} \left(\beta_0^{-\frac{1}{2}} (\beta_0 + \beta_1) |\boldsymbol{\theta}|_{H^{k+2}(\mathcal{T}_h)^2} + \mu^{-\frac{1}{2}} |\boldsymbol{\gamma}|_{H^{k+1}(\mathcal{T}_h)^2} \right). \tag{32}$$

Remark 5 (Regularity of the shear strain $\boldsymbol{\gamma}$). Under the regularity assumptions on u and $\boldsymbol{\theta}$ in the theorem, the shear strain defined by (1c) satisfies $\boldsymbol{\gamma} \in H^1(\Omega)^2 \cap H^{k+1}(\mathcal{T}_h)^2$.

Proof. See Section 4.3. □

The bound (32) shows that the DDR scheme achieves as expected a high-order of accuracy, when the solution is smooth enough and t is not too small. When $t \to 0$ the higher derivatives of the shear strain $\boldsymbol{\gamma}$ are known to explode; typically, $|\boldsymbol{\gamma}|_{H^{k+1}(\mathcal{T}_h)^2}$ grows as t^{-k-1}, as explained in [5, Theorem 2.1 and following remarks]. Thus, even though t does not explicitly appear in the right-hand side of (32), the dependency of this right-hand side on higher derivatives of the solution means that this estimate is not locking-free. Such a dependency is unavoidable for high-order schemes (see, e.g., [4] in the case of continuous/discontinuous Galerkin schemes). However, for $k = 0$, one could expect a better estimate than (32) in which $|\boldsymbol{\gamma}|_{H^1(\mathcal{T}_h)}$ is multiplied by t as in [4, 11, 17, 28]; this ensures that the method is locking-free at least if Ω is convex since, on such domains, $t|\boldsymbol{\gamma}|_{H^1(\Omega)}$ remains bounded as $t \to 0$. Such an error estimate is stated in the next theorem. Note that, contrary to most analyses in the aforementioned references and others (a notable exception being [11]), the proof of the following estimate does not use a Helmoltz decomposition of the shear strain.

Theorem 6 (Locking-free error estimate for $k = 0$)**.** *Assume the hypotheses of Theorem 4, and that $k = 0$. Then, it holds*

$$\|(\underline{\boldsymbol{\theta}}_h - \underline{\boldsymbol{I}}^0_{\boldsymbol{\Theta},h}\boldsymbol{\theta}, \underline{u}_h - \underline{I}^0_{U,h}u)\|_{\boldsymbol{\Theta}\times U,h} \\ \lesssim h\left(\beta_0^{-\frac{1}{2}}(\beta_0+\beta_1)|\boldsymbol{\theta}|_{H^2(\mathcal{T}_h)^2} + \kappa^{-\frac{1}{2}}t|\boldsymbol{\gamma}|_{H^1(\mathcal{T}_h)^2} + \beta_0^{-\frac{1}{2}}\|\boldsymbol{\gamma}\|_{L^2(\Omega)^2} + \mu^{-\frac{1}{2}}\|f\|_{L^2(\Omega)}\right). \quad (33)$$

Proof. See Section 4.4. □

Remark 7 (Locking-free property). If Ω is convex, all terms in the right-hand side of (33) are bounded independently of t [5, Theorem 2.1]. The techniques used to prove (33) can be extended (at the price of some technicalities) to arbitrary values of k to replace, in the right-hand side of (32), the term $|\boldsymbol{\gamma}|_{H^{k+1}(\mathcal{T}_h)^2}$ with $t|\boldsymbol{\gamma}|_{H^{k+1}(\mathcal{T}_h)^2} + |\boldsymbol{\gamma}|_{H^k(\mathcal{T}_h)^2} + |f|_{H^k(\mathcal{T}_h)}$ in the spirit of [4, Remark 4.3]. However, since a bound independent of t for the quantity $t|\boldsymbol{\gamma}|_{H^{k+1}(\mathcal{T}_h)^2} + |\boldsymbol{\gamma}|_{H^k(\mathcal{T}_h)^2} + |f|_{H^k(\mathcal{T}_h)}$ can only be established for $k = 0$, this would not yield complete robustness of the estimate (32) for $k \geq 1$. For this reason, and also to make the exposition less technical, we have decided to state two separate estimates.

4.3 Proof of the arbitrary-order error estimate

Proof of Theorem 4. 1. *Basic error estimate.* Combining the coercivity (29) of A_h with the Third Strang Lemma [18, Theorem 10], we obtain the following basic error estimate:

$$\|(\underline{\boldsymbol{\theta}}_h - \underline{\boldsymbol{I}}^k_{\boldsymbol{\Theta},h}\boldsymbol{\theta}, \underline{u}_h - \underline{I}^k_{U,h}u)\|_{\boldsymbol{\Theta}\times U,h} \lesssim \sup_{(\underline{\boldsymbol{\eta}}_h,\underline{v}_h)\in\underline{\boldsymbol{\Theta}}^k_{h,0}\times\underline{U}^k_{h,0}\setminus\{(\underline{\boldsymbol{0}},\underline{0})\}} \frac{\mathcal{E}_h((\boldsymbol{\theta},u);(\underline{\boldsymbol{\eta}}_h,\underline{v}_h))}{\|(\underline{\boldsymbol{\eta}}_h,\underline{v}_h)\|_{\boldsymbol{\Theta}\times U,h}}, \quad (34)$$

where the consistency error linear form $\mathcal{E}_h((\boldsymbol{\theta},u);\cdot)$ is such that, for all $(\underline{\boldsymbol{\eta}}_h,\underline{v}_h) \in \underline{\boldsymbol{\Theta}}^k_{h,0}\times\underline{U}^k_{h,0}$,

$$\mathcal{E}_h((\boldsymbol{\theta},u);(\underline{\boldsymbol{\eta}}_h,\underline{v}_h)) := \ell_h(\underline{v}_h) - \mathrm{A}_h((\underline{\boldsymbol{I}}^k_{\boldsymbol{\Theta},h}\boldsymbol{\theta}, \underline{I}^k_{U,h}u),(\underline{\boldsymbol{\eta}}_h,\underline{v}_h)). \quad (35)$$

2. *Reformulation of the consistency error.* To prove (32), we need to estimate the dual norm of the consistency error, which corresponds to the right-hand side of (34). We first recast b_h. Recall the definition (9) of the modified interpolator $\underline{\boldsymbol{I}}^{\flat,k}_{\boldsymbol{\Theta},h}$ and notice that, by Remark 2, it holds

$$(\underline{\boldsymbol{I}}^k_{\boldsymbol{\Theta},h}\boldsymbol{\eta},\underline{\boldsymbol{\tau}}_h)_{\boldsymbol{\Theta},h} = (\underline{\boldsymbol{I}}^{\flat,k}_{\boldsymbol{\Theta},h}\boldsymbol{\eta},\underline{\boldsymbol{\tau}}_h)_{\boldsymbol{\Theta},h} \qquad \forall(\boldsymbol{\eta},\underline{\boldsymbol{\tau}}_h)\in H^1(\Omega)^2\times\underline{\boldsymbol{\Theta}}^k_h. \quad (36)$$

We can then write

$$\begin{aligned}\mathrm{b}_h((\underline{\boldsymbol{I}}^k_{\boldsymbol{\Theta},h}\boldsymbol{\theta}, \underline{I}^k_{U,h}u),(\underline{\boldsymbol{\eta}}_h,\underline{v}_h)) &= \frac{\kappa}{t^2}(\underline{\boldsymbol{I}}^{\flat,k}_{\boldsymbol{\Theta},h}\boldsymbol{\theta} - \underline{\boldsymbol{G}}^k_h(\underline{I}^k_{U,h}u), \underline{\boldsymbol{\eta}}_h - \underline{\boldsymbol{G}}^k_h\underline{v}_h)_{\boldsymbol{\Theta},h}\\ &= \frac{\kappa}{t^2}(\underline{\boldsymbol{I}}^{\flat,k}_{\boldsymbol{\Theta},h}(\boldsymbol{\theta} - \mathbf{grad}\,u), \underline{\boldsymbol{\eta}}_h - \underline{\boldsymbol{G}}^k_h\underline{v}_h)_{\boldsymbol{\Theta},h}\\ &= (\underline{\boldsymbol{I}}^k_{\boldsymbol{\Theta},h}\boldsymbol{\gamma}, \underline{\boldsymbol{G}}^k_h\underline{v}_h - \underline{\boldsymbol{\eta}}_h)_{\boldsymbol{\Theta},h},\end{aligned}$$

where we have used the definition (23) of b_h along with (36) in the first line, the key commutation property (10) to pass to the second line, and the definition (1c) of the shear strain $\boldsymbol{\gamma}$ followed by (36) to conclude. Expanding the inner product $(\cdot,\cdot)_{\boldsymbol{\Theta},h}$ according to its definition from the local products (24) and using the relation $\boldsymbol{P}^k_{\boldsymbol{\Theta},T}\underline{\boldsymbol{G}}^k_T = \boldsymbol{G}^k_T$ (see [19, Proposition 15]), we infer

$$\mathrm{b}_h((\underline{\boldsymbol{I}}^k_{\boldsymbol{\Theta},h}\boldsymbol{\theta}, \underline{I}^k_{U,h}u),(\underline{\boldsymbol{\eta}}_h,\underline{v}_h)) = \sum_{T\in\mathcal{T}_h}\int_T \boldsymbol{\gamma}\cdot(\boldsymbol{G}^k_T\underline{v}_T - \boldsymbol{P}^k_{\boldsymbol{\Theta},T}\underline{\boldsymbol{\eta}}_T) - \mathfrak{T} \quad (37)$$

with

$$\mathfrak{T} := \sum_{T\in\mathcal{T}_h}\int_T [\boldsymbol{\gamma} - \boldsymbol{P}^k_{\boldsymbol{\Theta},T}(\underline{\boldsymbol{I}}^k_{\boldsymbol{\Theta},T}\boldsymbol{\gamma})]\cdot \boldsymbol{P}^k_{\boldsymbol{\Theta},T}(\underline{\boldsymbol{G}}^k_T\underline{v}_T - \underline{\boldsymbol{\eta}}_T) + \sum_{T\in\mathcal{T}_h}\mathrm{S}_{\boldsymbol{\Theta},T}(\underline{\boldsymbol{I}}^k_{\boldsymbol{\Theta},T}\boldsymbol{\gamma}, \underline{\boldsymbol{G}}^k_T\underline{v}_T - \underline{\boldsymbol{\eta}}_T).$$

Accounting for the definition of the material tensor $\mathbf{C}$, we also have, for all $\underline{\boldsymbol{\tau}}_h, \underline{\boldsymbol{\eta}}_h \in \underline{\boldsymbol{\Theta}}^k_h$,

$$\mathrm{a}_h(\underline{\boldsymbol{\tau}}_h, \underline{\boldsymbol{\eta}}_h) = \int_\Omega \mathbf{C}\mathbf{G}^k_{\mathrm{s},h}\underline{\boldsymbol{\tau}}_h : \mathbf{G}^k_{\mathrm{s},h}\underline{\boldsymbol{\eta}}_h + \beta_0\mathrm{s}_h(\underline{\boldsymbol{\tau}}_h, \underline{\boldsymbol{\eta}}_h) + \beta_0\mathrm{j}_h(\underline{\boldsymbol{\tau}}_h, \underline{\boldsymbol{\eta}}_h). \tag{38}$$

Recalling the definitions (22) of A_h and ℓ_h, the relations $\boldsymbol{\gamma} = -\,\mathbf{div}(\mathbf{C}\,\mathbf{grad}_{\mathrm{s}}\,\boldsymbol{\theta})$ and $f = -\operatorname{div}\boldsymbol{\gamma}$ (see (1a) and (1b)) along with (37) and (38) shows that the consistency error (35) can be recast as

$$\mathcal{E}_h((\boldsymbol{\theta}, u); (\underline{\boldsymbol{\eta}}_h, \underline{v}_h)) = \mathcal{E}_{\mathbf{grad},h}(\boldsymbol{\gamma}; \underline{v}_h) + \mathfrak{T} + \mathcal{E}_{\mathbf{grad}_{\mathrm{s}},h}(\mathbf{C}\,\mathbf{grad}_{\mathrm{s}}\,\boldsymbol{\theta}; \underline{\boldsymbol{\eta}}_h), \tag{39}$$

where the adjoint consistency errors for the gradient on $\underline{U}^k_h$ and for the symmetric gradient on $\boldsymbol{\Theta}^k_h$ are defined as

$$\begin{aligned}
\mathcal{E}_{\mathbf{grad},h}(\boldsymbol{\gamma}; \underline{v}_h) &:= -\int_\Omega \operatorname{div}\boldsymbol{\gamma}\; P^{k+1}_{U,h}\underline{v}_h - \sum_{T\in\mathcal{T}_h}\int_T \boldsymbol{\gamma}\cdot\boldsymbol{G}^k_T\underline{v}_T,\\
\mathcal{E}_{\mathbf{grad}_{\mathrm{s}},h}(\mathbf{C}\,\mathbf{grad}_{\mathrm{s}}\,\boldsymbol{\theta}; \underline{\boldsymbol{\eta}}_h) &:= -\sum_{T\in\mathcal{T}_h}\int_T \mathbf{div}(\mathbf{C}\,\mathbf{grad}_{\mathrm{s}}\,\boldsymbol{\theta})\cdot\boldsymbol{P}^k_{\boldsymbol{\Theta},T}\underline{\boldsymbol{\eta}}_T - \int_\Omega \mathbf{C}\mathbf{G}^k_{\mathrm{s},h}(\underline{\boldsymbol{I}}^k_{\boldsymbol{\Theta},h}\boldsymbol{\theta}) : \mathbf{G}^k_{\mathrm{s},h}\underline{\boldsymbol{\eta}}_h\\
&\quad - \beta_0\mathrm{s}_h(\underline{\boldsymbol{I}}^k_{\boldsymbol{\Theta},h}\boldsymbol{\theta}, \underline{\boldsymbol{\eta}}_h) - \beta_0\mathrm{j}_h(\underline{\boldsymbol{I}}^k_{\boldsymbol{\Theta},h}\boldsymbol{\theta}, \underline{\boldsymbol{\eta}}_h).
\end{aligned}$$

3. *Bound on the consistency error*. To deal with $\mathcal{E}_{\mathbf{grad}_{\mathrm{s}},h}$, we use the estimate in [20, Lemma 7.27] (and [20, Lemma 7.43] if $k = 0$) which, in the present context, yields

$$\begin{aligned}
|\mathcal{E}_{\mathbf{grad}_{\mathrm{s}},h}(\mathbf{C}\,\mathbf{grad}_{\mathrm{s}}\,\boldsymbol{\theta}; \underline{\boldsymbol{\eta}}_h)| &\lesssim h^{k+1}(\beta_0+\beta_1)|\boldsymbol{\theta}|_{H^{k+2}(\mathcal{T}_h)^2}\left(\|\mathbf{G}^k_{\mathrm{s},h}\underline{\boldsymbol{\eta}}_h\|^2_{L^2(\Omega)^{2\times 2}} + |\underline{\boldsymbol{\eta}}_h|^2_{\mathrm{s,j},h}\right)^{\frac12}\\
&\lesssim h^{k+1}\beta_0^{-\frac12}(\beta_0+\beta_1)|\boldsymbol{\theta}|_{H^{k+2}(\mathcal{T}_h)^2}\|(\underline{\boldsymbol{\eta}}_h, \underline{v}_h)\|_{\boldsymbol{\Theta}\times U,h},
\end{aligned} \tag{40}$$

where the conclusion follows from the definition (27) of the discrete norm.

The term $\mathfrak{T}$ is estimated using Cauchy–Schwarz inequalities:

$$\begin{aligned}
|\mathfrak{T}| &\le \sum_{T\in\mathcal{T}_h}\|\boldsymbol{\gamma} - \boldsymbol{P}^k_{\boldsymbol{\Theta},T}(\underline{\boldsymbol{I}}^k_{\boldsymbol{\Theta},T}\boldsymbol{\gamma})\|_{L^2(T)^2}\,\|\boldsymbol{P}^k_{\boldsymbol{\Theta},T}(\underline{\boldsymbol{G}}^k_T\underline{v}_T - \underline{\boldsymbol{\eta}}_T)\|_{L^2(T)^2}\\
&\quad + \sum_{T\in\mathcal{T}_h}\mathrm{S}_{\boldsymbol{\Theta},T}(\underline{\boldsymbol{I}}^k_{\boldsymbol{\Theta},T}\boldsymbol{\gamma}, \underline{\boldsymbol{I}}^k_{\boldsymbol{\Theta},T}\boldsymbol{\gamma})^{\frac12}\,\mathrm{S}_{\boldsymbol{\Theta},T}(\underline{\boldsymbol{G}}^k_T\underline{v}_T - \underline{\boldsymbol{\eta}}_T, \underline{\boldsymbol{G}}^k_T\underline{v}_T - \underline{\boldsymbol{\eta}}_T)^{\frac12}\\
&\lesssim \sum_{T\in\mathcal{T}_h} h^{k+1}|\boldsymbol{\gamma}|_{H^{k+1}(T)^2}\left(\|\boldsymbol{P}^k_{\boldsymbol{\Theta},T}(\underline{\boldsymbol{G}}^k_T\underline{v}_T - \underline{\boldsymbol{\eta}}_T)\|_{L^2(T)^2} + \mathrm{S}_{\boldsymbol{\Theta},T}(\underline{\boldsymbol{G}}^k_T\underline{v}_T - \underline{\boldsymbol{\eta}}_T, \underline{\boldsymbol{G}}^k_T\underline{v}_T - \underline{\boldsymbol{\eta}}_T)^{\frac12}\right)\\
&\lesssim h^{k+1}|\boldsymbol{\gamma}|_{H^{k+1}(\mathcal{T}_h)^2}\|\underline{\boldsymbol{G}}^k_h\underline{v}_h - \underline{\boldsymbol{\eta}}_h\|_{\boldsymbol{\Theta},h},
\end{aligned}$$

where we have used, in the second line, the consistency properties of $\boldsymbol{P}^k_{\boldsymbol{\Theta},T}\underline{\boldsymbol{I}}^k_{\boldsymbol{\Theta},T}$ and $\mathrm{S}_{\boldsymbol{\Theta},T}$ (two-dimensional versions of [19, Eqs. (6.3) and (6.9)], see Remark 8 below), and the conclusion follows from Cauchy–Schwarz inequalities on the sum and the definition of the norm $\|\cdot\|_{\boldsymbol{\Theta},h}$. Using the definition (27) of the discrete norm, we infer

$$|\mathfrak{T}| \lesssim h^{k+1}\kappa^{-\frac12}t|\boldsymbol{\gamma}|_{H^{k+1}(\mathcal{T}_h)^2}\|(\underline{\boldsymbol{\eta}}_h, \underline{v}_h)\|_{\boldsymbol{\Theta}\times U,h}. \tag{41}$$

The estimate of $\mathcal{E}_{\mathbf{grad},h}$ follows proceeding as in the proof of [19, Theorem 39], with straightforward modifications to account for the different boundary conditions, fewer (and simpler) terms to track, and accounting for Remark 8:

$$|\mathcal{E}_{\mathbf{grad},h}(\boldsymbol{\gamma};\underline{v}_h)| \lesssim h^{k+1}|\boldsymbol{\gamma}|_{H^{k+1}(\mathcal{T}_h)^2}\|\underline{\boldsymbol{G}}_h^k\underline{v}_h\|_{\boldsymbol{\Theta},h} \le h^{k+1}\mu^{-\frac{1}{2}}|\boldsymbol{\gamma}|_{H^{k+1}(\mathcal{T}_h)^2}\|(\underline{\boldsymbol{\eta}}_h,\underline{v}_h)\|_{\boldsymbol{\Theta}\times U,h}. \tag{42}$$

4. *Conclusion.* Plugging the estimates (40), (41) and (42) into (39), we arrive at

$$\begin{aligned}&|\mathcal{E}_h((\boldsymbol{\theta},u);(\underline{\boldsymbol{\eta}}_h,\underline{v}_h))|\\ &\qquad\lesssim h^{k+1}\left(\beta_0^{-\frac{1}{2}}(\beta_0+\beta_1)|\boldsymbol{\theta}|_{H^{k+2}(\mathcal{T}_h)^2}+\kappa^{-\frac{1}{2}}t|\boldsymbol{\gamma}|_{H^{k+1}(\mathcal{T}_h)^2}+\mu^{-\frac{1}{2}}|\boldsymbol{\gamma}|_{H^{k+1}(\mathcal{T}_h)^2}\right)\|(\underline{\boldsymbol{\eta}}_h,\underline{v}_h)\|_{\boldsymbol{\Theta}\times U,h}.\end{aligned}$$

The estimate (32) follows using this bound in (34) and recalling that $\mu \le \kappa$ and $t \le 1$. □

Remark 8 (Norms of $\boldsymbol{\gamma}$ in the estimates). In [19], the estimates mentioned above (Theorem 39 and Section 6.1) involve, in the case $k = 0$, weighted H^2-seminorms of $\boldsymbol{\gamma}$. This is because these estimates are stated in three dimensions, in which interpolating a function on $\underline{\boldsymbol{\Theta}}_h^k$ requires a higher minimal regularity (to ensure traces along the edges are well-defined). In two dimensions, the local interpolator obtained restricting (7) to T is well-defined on $H^1(T)^2$, and the seminorm in this space is sufficient to state the consistency estimates for $k = 0$.

4.4 Proof of the low-order locking-free error estimate

The proof of Theorem 6 relies on liftings of elements in $\underline{U}_T^0$ and $\underline{\boldsymbol{\Theta}}_T^0$, for each $T \in \mathcal{T}_h$. The assumption on the mesh yields a conforming simplicial subdivision $\mathcal{S}_T$ of T that is shape regular (with the same regularity parameter as in the mesh regularity assumption); actually, by [20, Assumption 7.6] each $T \in \mathcal{T}_h$ is star-shaped with respect to every point in a ball of radius ϱh_T, where ϱ is the mesh regularity parameter, so $\mathcal{S}_T$ can be constructed by adding only one vertex (the center of that ball) in T and creating the triangles between this vertex and the edges of T. The proof given here, however, applies also to elements that are possibly not star-shaped.

The coordinate $\boldsymbol{x}_V$ of any vertex V of $\mathcal{S}_T$ can be written as a convex combination of the coordinates of the vertices $\mathcal{V}_T$ of T:

$$\boldsymbol{x}_V = \sum_{W\in\mathcal{V}_T}\lambda_{V,W}\boldsymbol{x}_W\,, \qquad \text{with } \lambda_{V,W} \ge 0 \text{ and } \sum_{W\in\mathcal{V}_T}\lambda_{V,W} = 1 \tag{43}$$

(this includes the vertices $V \in \mathcal{V}_T$, in which case we choose $\lambda_{V,V} = 1$ and $\lambda_{V,W} = 0$ if $W \ne V$). Denoting by $\mathcal{P}_c^1(\mathcal{S}_T)$ the space of $H^1(T)$-conforming piecewise $\mathcal{P}^1$ functions on $\mathcal{S}_T$, for all $\underline{z}_T = z_{\mathcal{E}_T} \in \underline{U}_T^0$ we define $\widetilde{z}_T \in \mathcal{P}_c^1(\mathcal{S}_T)$ such that

$$\widetilde{z}_T(\boldsymbol{x}_V) = \sum_{W\in\mathcal{V}_T}\lambda_{V,W}\, z_{\mathcal{E}_T}(\boldsymbol{x}_W).$$

This construction is linearly exact, that is

$$\widetilde{\underline{I}_{U,T}^0\phi_T} = \phi_T \qquad \forall\phi_T \in \mathcal{P}^1(T). \tag{44}$$

The next lemma, whose proof is postponed to the end of the section, states useful properties of the lifting $\underline{U}_T^0 \ni \underline{z}_T \mapsto \widetilde{z}_T \in \mathcal{P}_c^1(\mathcal{S}_T)$.

Lemma 9 (Properties of the lifting on $\underline{U}_T^0$)**.** *The following properties hold: For all* $\underline{z}_T \in \underline{U}_T^0$,

$$\boldsymbol{\pi}^0_{\mathcal{P},T}(\mathbf{grad}\,\widetilde{z}_T) = \boldsymbol{G}^0_T \underline{z}_T, \tag{45}$$

$$\|\,\mathbf{grad}\,\widetilde{z}_T\|_{L^2(T)^2} \lesssim \|\underline{\boldsymbol{G}}^0_T \underline{z}_T\|_{\boldsymbol{\Theta},T}, \tag{46}$$

$$\|\widetilde{z}_T - P^1_{U,T}\underline{z}_T\|_{L^2(T)} \lesssim h_T \|\underline{\boldsymbol{G}}^0_T \underline{z}_T\|_{\boldsymbol{\Theta},T}, \tag{47}$$

where $\|\cdot\|_{\boldsymbol{\Theta},T}$ *is the local seminorm induced by the product* (24) *on* $\underline{\boldsymbol{\Theta}}_T^0$*. Moreover, if* $\underline{z}_h \in \underline{U}^0_{h,0}$ *and* $\widetilde{z}_h$ *is defined such that* $(\widetilde{z}_h)_{|T} = \widetilde{z}_T$ *for all* $T \in \mathcal{T}_h$*, then* $\widetilde{z}_h \in H^1_0(\Omega)$.

We now define the lifting on $\underline{\boldsymbol{\Theta}}_T^0$. For any $\underline{\boldsymbol{\eta}}_T = (\boldsymbol{\eta}_E)_{E\in\mathcal{E}_T} \in \underline{\boldsymbol{\Theta}}_T^0$, let $\underline{\boldsymbol{\eta}}_T^\flat = ((\boldsymbol{\eta}_E \cdot \boldsymbol{t}_E)\boldsymbol{t}_E)_{E\in\mathcal{E}_T}$ be the vector comprising only the tangential components to the edges. Since $(\cdot,\cdot)_{\boldsymbol{\Theta},T}$ is an inner product when only these components are considered, we can write a unique decomposition

$$\underline{\boldsymbol{\eta}}_T^\flat = \underline{\boldsymbol{G}}^0_T \underline{w}_T + \underline{\boldsymbol{\kappa}}_T \text{ with } \underline{w}_T \in \underline{U}_T^0 \text{ and } \underline{\boldsymbol{\kappa}}_T \perp \underline{\boldsymbol{G}}^0_T \underline{U}_T^0,$$

the orthogonality being understood for $(\cdot,\cdot)_{\boldsymbol{\Theta},T}$. We then set

$$\widetilde{\boldsymbol{\eta}}_T \coloneqq \mathbf{grad}\,\widetilde{w}_T + \boldsymbol{P}^0_{\boldsymbol{\Theta},T}\underline{\boldsymbol{\kappa}}_T.$$

The proof of the properties of the lifting $\underline{\boldsymbol{\Theta}}_T^0 \ni \underline{\boldsymbol{\eta}}_T \mapsto \widetilde{\boldsymbol{\eta}}_T \in L^2(T)^2$ stated in the following lemma is postponed to the end of the section.

Lemma 10 (Properties of the lifting on $\underline{\boldsymbol{\Theta}}_T^0$)**.** *The following properties hold: For all* $\underline{\boldsymbol{\eta}}_T \in \underline{\boldsymbol{\Theta}}_T^0$,

$$\boldsymbol{\pi}^0_{\mathcal{P},T}\widetilde{\boldsymbol{\eta}}_T = \boldsymbol{P}^0_{\boldsymbol{\Theta},T}\underline{\boldsymbol{\eta}}_T, \tag{48}$$

$$\|\,\mathbf{grad}\,\widetilde{v}_T - \widetilde{\boldsymbol{\eta}}_T\|_{L^2(T)^2} \lesssim \|\underline{\boldsymbol{G}}^0_T \underline{v}_T - \underline{\boldsymbol{\eta}}_T\|_{\boldsymbol{\Theta},T} \qquad \forall \underline{v}_T \in \underline{U}_T^0. \tag{49}$$

Moreover, for all $\underline{\boldsymbol{\eta}}_h \in \underline{\boldsymbol{\Theta}}^0_{h,0}$,

$$\left(\sum_{T\in\mathcal{T}_h} \|\widetilde{\boldsymbol{\eta}}_T - \boldsymbol{P}^0_{\boldsymbol{\Theta},T}\underline{\boldsymbol{\eta}}_T\|^2_{L^2(T)^2}\right)^{\frac{1}{2}} \lesssim h\left(\|\mathbf{G}^0_{\mathrm{s},h}\underline{\boldsymbol{\eta}}_h\|^2_{L^2(\Omega)^{2\times 2}} + |\underline{\boldsymbol{\eta}}_h|^2_{\mathrm{s,j},h}\right)^{\frac{1}{2}}. \tag{50}$$

We are now ready to prove Theorem 6.

Proof of Theorem 6. Given the basic error estimate (34), we only have to find a proper upper bound of the consistency error. We consider the first term in the expression (37) of $\mathrm{b}_h((\underline{\boldsymbol{I}}^k_{\boldsymbol{\Theta},h}\boldsymbol{\theta}, \underline{I}^k_{U,h}u), (\underline{\boldsymbol{\eta}}_h, \underline{v}_h))$. Owing to (45) and (48) we have

$$\begin{aligned}
\int_T \boldsymbol{\gamma}\cdot(\boldsymbol{G}^0_T\underline{v}_T - \boldsymbol{P}^0_{\boldsymbol{\Theta},T}\underline{\boldsymbol{\eta}}_T) &= \int_T \boldsymbol{\gamma}\cdot\boldsymbol{\pi}^0_{\mathcal{P},T}(\mathbf{grad}\,\widetilde{v}_T - \widetilde{\boldsymbol{\eta}}_T) = \int_T \boldsymbol{\pi}^0_{\mathcal{P},T}\boldsymbol{\gamma}\cdot(\mathbf{grad}\,\widetilde{v}_T - \widetilde{\boldsymbol{\eta}}_T)\\
&= \int_T \boldsymbol{\gamma}\cdot(\mathbf{grad}\,\widetilde{v}_T - \widetilde{\boldsymbol{\eta}}_T) + \underbrace{\int_T (\boldsymbol{\pi}^0_{\mathcal{P},T}\boldsymbol{\gamma} - \boldsymbol{\gamma})\cdot(\mathbf{grad}\,\widetilde{v}_T - \widetilde{\boldsymbol{\eta}}_T)}_{=:\mathfrak{T}_{T,a}}\\
&= \int_T \boldsymbol{\gamma}\cdot\mathbf{grad}\,\widetilde{v}_T - \int_T \boldsymbol{\gamma}\cdot\boldsymbol{P}^0_{\boldsymbol{\Theta},T}\underline{\boldsymbol{\eta}}_T + \underbrace{\int_T \boldsymbol{\gamma}\cdot(\boldsymbol{P}^0_{\boldsymbol{\Theta},T}\underline{\boldsymbol{\eta}}_T - \widetilde{\boldsymbol{\eta}}_T)}_{=:\mathfrak{T}_{T,b}} + \mathfrak{T}_{T,a}.
\end{aligned}$$

Summing over $T \in \mathcal{T}_h$, using the fact that $\widetilde{v}_h \in H_0^1(\Omega)$ (see Lemma 9) to perform an integration by parts, recalling that $f = -\operatorname{div}\boldsymbol{\gamma}$ by (1b), and setting $\mathfrak{T}_\star := \sum_{T\in\mathcal{T}_h} \mathfrak{T}_{T,\star}$ for $\star \in \{a, b\}$, we infer

$$\begin{aligned}\sum_{T\in\mathcal{T}_h}\int_T \boldsymbol{\gamma}\cdot(\boldsymbol{G}_T^0\underline{v}_T - \boldsymbol{P}_{\boldsymbol{\Theta},T}^0\underline{\boldsymbol{\eta}}_T) &= \int_\Omega f\,\widetilde{v}_h - \sum_{T\in\mathcal{T}_h}\int_T \boldsymbol{\gamma}\cdot\boldsymbol{P}_{\boldsymbol{\Theta},T}^0\underline{\boldsymbol{\eta}}_T + \mathfrak{T}_a + \mathfrak{T}_b\\ &= \int_\Omega f\,P_{U,h}^1\underline{v}_h - \sum_{T\in\mathcal{T}_h}\int_T \boldsymbol{\gamma}\cdot\boldsymbol{P}_{\boldsymbol{\Theta},T}^0\underline{\boldsymbol{\eta}}_T + \underbrace{\int_\Omega f(\widetilde{v}_h - P_{U,h}^1\underline{v}_h)}_{=:\mathfrak{T}_c} + \mathfrak{T}_a + \mathfrak{T}_b.\end{aligned}$$

We plug this relation into the expression (37) of $\mathrm{b}_h((\underline{\boldsymbol{I}}_{\boldsymbol{\Theta},h}^k\boldsymbol{\theta}, \underline{I}_{U,h}^k u), (\underline{\boldsymbol{\eta}}_h, \underline{v}_h))$ and recall (38) and the definitions (22) of A_h and ℓ_h to re-write consistency error (35) as

$$\mathcal{E}_h((\boldsymbol{\theta}, u); (\underline{\boldsymbol{\eta}}_h, \underline{v}_h)) = \mathcal{E}_{\mathbf{grad}_{\mathrm{s}},h}(\mathbf{C}\,\mathbf{grad}_{\mathrm{s}}\,\boldsymbol{\theta}; \underline{\boldsymbol{\eta}}_h) - \mathfrak{T}_a - \mathfrak{T}_b - \mathfrak{T}_c + \mathfrak{T}. \tag{51}$$

We now estimate $\mathfrak{T}_a$, $\mathfrak{T}_b$ and $\mathfrak{T}_c$. Using the approximation properties of $\boldsymbol{\pi}_{\mathcal{P},T}^0$ together with Cauchy–Schwarz inequalities and (49), we have

$$|\mathfrak{T}_a| \lesssim h|\boldsymbol{\gamma}|_{H^1(\mathcal{T}_h)^2}\|\underline{\boldsymbol{G}}_h^k\underline{v}_h - \underline{\boldsymbol{\eta}}_h\|_{\boldsymbol{\Theta},h} \lesssim h|\boldsymbol{\gamma}|_{H^1(\mathcal{T}_h)^2}\kappa^{-\frac{1}{2}}t\|(\underline{\boldsymbol{\eta}}_h, \underline{v}_h)\|_{\boldsymbol{\Theta}\times U,h}, \tag{52}$$

where we have used the definition (27) of $\|\cdot\|_{\boldsymbol{\Theta}\times U,h}$ to conclude. For $\mathfrak{T}_b$, we use again Cauchy–Schwarz inequalities and the estimate (50), together with the definition of the norm on $\underline{\boldsymbol{\Theta}}_{h,0}^0 \times \underline{U}_{h,0}^0$, to write

$$|\mathfrak{T}_b| \lesssim \|\boldsymbol{\gamma}\|_{L^2(\Omega)^2} h\beta_0^{-\frac{1}{2}}\|(\underline{\boldsymbol{\eta}}_h, \underline{v}_h)\|_{\boldsymbol{\Theta}\times U,h}. \tag{53}$$

Finally, for $\mathfrak{T}_c$, Cauchy–Schwarz inequalities followed by the estimate (47) yield

$$|\mathfrak{T}_c| \lesssim \|f\|_{L^2(\Omega)} h\|\underline{\boldsymbol{G}}_h^0\underline{v}_h\|_{\boldsymbol{\Theta},h} \lesssim \|f\|_{L^2(\Omega)} h\mu^{-\frac{1}{2}}\|(\underline{\boldsymbol{\eta}}_h, \underline{v}_h)\|_{\boldsymbol{\Theta}\times U,h}. \tag{54}$$

Plugging (52)–(54) and the estimates (41) on $\mathfrak{T}$ and (40) on $\mathcal{E}_{\mathbf{grad}_{\mathrm{s}},h}(\mathbf{C}\,\mathbf{grad}_{\mathrm{s}}\,\boldsymbol{\theta}; \underline{\boldsymbol{\eta}}_h)$ into (51), we infer

$$\begin{aligned}&|\mathcal{E}_h((\boldsymbol{\theta}, u); (\underline{\boldsymbol{\eta}}_h, \underline{v}_h))|\\ &\lesssim h\left(\kappa^{-\frac{1}{2}}t|\boldsymbol{\gamma}|_{H^1(\mathcal{T}_h)^2} + \beta_0^{-\frac{1}{2}}\|\boldsymbol{\gamma}\|_{L^2(\Omega)^2} + \mu^{-\frac{1}{2}}\|f\|_{L^2(\Omega)} + \beta_0^{-\frac{1}{2}}(\beta_0+\beta_1)|\boldsymbol{\theta}|_{H^2(\mathcal{T}_h)^2}\right)\|(\underline{\boldsymbol{\eta}}_h, \underline{v}_h)\|_{\boldsymbol{\Theta}\times U,h}.\end{aligned}$$

Plugging this estimate into (34) concludes the proof. □

To conclude this section, we provide the proofs of the properties of the liftings.

Proof of Lemma 9. 1. *Proof of* (45). Let $\underline{z}_T \in \underline{U}_T^0$. For all $\boldsymbol{\eta} \in \boldsymbol{\mathcal{P}}^0(T)$, an integration by parts yields

$$\int_T \mathbf{grad}\,\widetilde{z}_T\cdot\boldsymbol{\eta} = \sum_{E\in\mathcal{E}_T}\int_E \widetilde{z}_T(\boldsymbol{\eta}\cdot\boldsymbol{n}_{TE}) = \sum_{E\in\mathcal{E}_T}\int_E z_{\mathcal{E}_T}(\boldsymbol{\eta}\cdot\boldsymbol{n}_{TE}) = \int_T \boldsymbol{G}_T^0\underline{z}_T\cdot\boldsymbol{\eta},$$

where the second equality comes from the definition of $\widetilde{z}_T$ which ensures that $(\widetilde{z}_T)_{|E} = (z_{\mathcal{E}_T})_{|E}$ for all $E \in \mathcal{E}_T$ (both functions are linear on E and match at the edge's vertices), and the last equality is obtained applying the definition (8) of $\boldsymbol{G}_T^0$. This proves (45).

2. *Proof of* (46). For any two vertices $V, V^\star$ of $\mathcal{S}_T$ we have by construction

$$\widetilde{z}_T(\boldsymbol{x}_V) - \widetilde{z}_T(\boldsymbol{x}_{V^\star}) = \sum_{W,Z\in\mathcal{V}_T}\lambda_{V,W}\lambda_{V^\star,Z}\left(z_{\mathcal{E}_T}(\boldsymbol{x}_W) - z_{\mathcal{E}_T}(\boldsymbol{x}_Z)\right).$$

Integrating the derivative (oriented by each tangent $\boldsymbol{t}_E$) of $z_{\mathcal{E}_T}$ on ∂T between W and Z and using the two-dimensional version of the equivalence stated in [19, Eq. (4.24)] between $\|\cdot\|_{\boldsymbol{\Theta},T}$ and the component L^2-norm, we have

$$|z_{\mathcal{E}_T}(\boldsymbol{x}_W) - z_{\mathcal{E}_T}(\boldsymbol{x}_Z)| \le \|z'_{\mathcal{E}_T}\|_{L^1(\partial T)} \le |\partial T|^{\frac{1}{2}} \|z'_{\mathcal{E}_T}\|_{L^2(\partial T)} \lesssim \|\underline{\boldsymbol{G}}^0_T \underline{z}_T\|_{\boldsymbol{\Theta},T}.$$

Since $\mathrm{card}(\mathcal{V}_T)$ is uniformly bounded by the mesh regularity parameter and $(\lambda_{V,W})_{W\in\mathcal{V}_T}$ and $(\lambda_{V^\star,Z})_{Z\in\mathcal{V}_T}$ are coefficients of convex combinations, we infer from the above relations that

$$|\widetilde{z}_T(\boldsymbol{x}_V) - \widetilde{z}_T(\boldsymbol{x}_{V^\star})| \lesssim \|\underline{\boldsymbol{G}}^0_T \underline{z}_T\|_{\boldsymbol{\Theta},T}.$$

Since any edge e of $\mathcal{S}_T$ has a length comparable to h_T, this shows that $|\,\mathbf{grad}\,\widetilde{z}_T \cdot \boldsymbol{t}_e| \lesssim h_T^{-1}\|\underline{\boldsymbol{G}}^0_T \underline{z}_T\|_{\boldsymbol{\Theta},T}$ where $\boldsymbol{t}_e$ is any unit tangent to e. Hence, on any triangle $\tau \in \mathcal{S}_T$,

$$\|\,\mathbf{grad}\,\widetilde{z}_T\|_{L^2(\tau)^2} = |\tau|^{\frac{1}{2}}|(\mathbf{grad}\,\widetilde{z}_T)_{|\tau}| \le |T|^{\frac{1}{2}}|(\mathbf{grad}\,\widetilde{z}_T)_{|\tau}| \lesssim |T|^{\frac{1}{2}} h_T^{-1}\|\underline{\boldsymbol{G}}^0_T \underline{z}_T\|_{\boldsymbol{\Theta},T}.$$

Using $|T|^{\frac{1}{2}} \lesssim h_T$, squaring, summing over $\tau \in \mathcal{S}_T$ and taking the square root concludes the proof of (46).

3. *Proof of* (47). We start from the following Poincaré inequality with trace:

$$\|w_T\|^2_{L^2(T)} \lesssim h_T^2 \|\,\mathbf{grad}\,w_T\|^2_{L^2(T)^2} + \sum_{E\in\mathcal{E}_T} h_E \|w_T\|^2_{L^2(E)} \qquad \forall w_T \in \mathcal{P}^1_{\mathrm{c}}(\mathcal{S}_T). \tag{55}$$

To prove this estimate, consider a triangle $\tau \in \mathcal{S}_T$ with an edge $e \subset \partial T$. Taking $\boldsymbol{x} \in \tau$ and $\boldsymbol{y} \in e$ we have $|w_T(\boldsymbol{x})| \le h_T|(\mathbf{grad}\,w_T)_{|\tau}| + |w_T(\boldsymbol{y})|$; integrating over $\boldsymbol{y} \in e$, squaring, integrating over $\boldsymbol{x} \in \tau$ and using $|\tau|/h_e \lesssim h_e$ (by shape regularity) leads to

$$\|w_T\|^2_{L^2(\tau)} \lesssim h_T^2 \|\,\mathbf{grad}\,w_T\|^2_{L^2(\tau)^2} + h_e \|w_T\|^2_{L^2(e)}. \tag{56}$$

If all triangles in $\mathcal{S}_T$ have an edge $e \subset \partial T$, summing (56) over $\tau \in \mathcal{S}_T$ concludes the proof of (55); otherwise, a discrete trace inequality and (56) give a bound on the trace of w_T on the other edges of τ, and the process can be iterated on the triangles in $\mathcal{S}_T$ that touch τ but do not have an edge on ∂T.

Applying (55) to $w_T = \widetilde{z}_T - P^1_{U,T}\underline{z}_T$, using a triangle inequality, $h_E \le h_T$, the estimate (46), and the fact that $(\widetilde{z}_T)_{|E} = (z_{\mathcal{E}_T})_{|E}$ for all $E \in \mathcal{E}_T$, we obtain

$$\|\widetilde{z}_T - P^1_{U,T}\underline{z}_T\|^2_{L^2(T)} \lesssim h_T^2 \left(\|\underline{\boldsymbol{G}}^0_T \underline{z}_T\|^2_{\boldsymbol{\Theta},T} + \|\,\mathbf{grad}\,P^1_{U,T}\underline{z}_T\|^2_{L^2(T)^2}\right) + h_T^2 \sum_{E\in\mathcal{E}_T} h_E^{-1}\|z_{\mathcal{E}_T} - P^1_{U,T}\underline{z}_T\|^2_{L^2(E)}.$$

The proof of (47) is completed by invoking [19, Lemma 35 and Eq. (4.24)] to write

$$\|\,\mathbf{grad}\,P^1_{U,T}\underline{z}_T\|^2_{L^2(T)^2} + \sum_{E\in\mathcal{E}_T} h_E^{-1}\|z_{\mathcal{E}_T} - P^1_{U,T}\underline{z}_T\|^2_{L^2(E)} \lesssim \|\underline{\boldsymbol{G}}^0_T \underline{z}_T\|^2_{\boldsymbol{\Theta},T}. \qquad \square$$

Proof of Lemma 10. 1. *Proof of* (48). By (45), $\boldsymbol{\pi}^0_{\mathcal{P},T}\widetilde{\boldsymbol{\eta}}_T = \boldsymbol{G}^0_T \underline{w}_T + \boldsymbol{P}^0_{\boldsymbol{\Theta},T}\underline{\boldsymbol{\kappa}}_T = \boldsymbol{P}^0_{\boldsymbol{\Theta},T}(\underline{\boldsymbol{G}}^0_T \underline{w}_T + \underline{\boldsymbol{\kappa}}_T)$, where the last equality follows from the relation $\boldsymbol{P}^0_{\boldsymbol{\Theta},T}\underline{\boldsymbol{G}}^0_T = \boldsymbol{G}^0_T$, see [19, Eq. (3.22)]. This proves that $\boldsymbol{\pi}^0_{\mathcal{P},T}\widetilde{\boldsymbol{\eta}}_T = \boldsymbol{P}^0_{\boldsymbol{\Theta},T}\underline{\boldsymbol{\eta}}^\flat_T$. Since $\boldsymbol{P}^0_{\boldsymbol{\Theta},T}$ depends only on the tangential components of $\underline{\boldsymbol{\eta}}_T$ (see (11) and (12)), this concludes the proof of (48).

2. *Proof of* (49). We use the definition of $\widetilde{\boldsymbol{\eta}}_T$ to write $\mathbf{grad}\,\widetilde{v}_T - \widetilde{\boldsymbol{\eta}}_T = \mathbf{grad}(\widetilde{v}_T - \widetilde{w}_T) - \boldsymbol{P}^0_{\boldsymbol{\Theta},T}\underline{\boldsymbol{\kappa}}_T$ and thus, by triangle inequality,

$$\begin{aligned}
\|\,\mathbf{grad}\,\widetilde{v}_T - \widetilde{\boldsymbol{\eta}}_T\|^2_{L^2(T)^2} &\le 2\|\,\mathbf{grad}(\widetilde{v}_T - \widetilde{w}_T)\|^2_{L^2(T)^2} + 2\|\boldsymbol{P}^0_{\boldsymbol{\Theta},T}\underline{\boldsymbol{\kappa}}_T\|^2_{L^2(T)^2} \\
&\lesssim \|\underline{\boldsymbol{G}}^0_T(\underline{v}_T - \underline{w}_T)\|^2_{\boldsymbol{\Theta},T} + \|\underline{\boldsymbol{\kappa}}_T\|^2_{\boldsymbol{\Theta},T} \\
&= \|\underline{\boldsymbol{G}}^0_T(\underline{v}_T - \underline{w}_T) - \underline{\boldsymbol{\kappa}}_T\|^2_{\boldsymbol{\Theta},T},
\end{aligned}$$

where the second line follows from (46) applied to $\underline{z}_T = \underline{v}_T - \underline{w}_T$ and the estimate $\|\boldsymbol{P}^0_{\boldsymbol{\Theta},T}\underline{\boldsymbol{\kappa}}_T\|_{L^2(T)^2} \lesssim \|\underline{\boldsymbol{\kappa}}_T\|_{\boldsymbol{\Theta},T}$ (see [19, Proposition 27]), while the conclusion is obtained using the orthogonality for the $(\cdot,\cdot)_{\boldsymbol{\Theta},T}$ product of $\underline{\boldsymbol{\kappa}}_T$ and $\underline{\boldsymbol{G}}^0_T(\underline{v}_T - \underline{w}_T)$. This gives

$$\|\,\mathbf{grad}\,\widetilde{v}_T - \widetilde{\boldsymbol{\eta}}_T\|_{L^2(T)^2} \lesssim \|\underline{\boldsymbol{G}}^0_T\underline{v}_T - \underline{\boldsymbol{\eta}}^\flat_T\|_{\boldsymbol{\Theta},T}$$

and the proof of (49) is complete since $\|\cdot\|_{\boldsymbol{\Theta},T}$ depends only on tangential components of vectors in $\underline{\boldsymbol{\Theta}}^0_T$.

3. *Proof of* (50). Let $\phi_T(\boldsymbol{x}) := \boldsymbol{P}^0_{\boldsymbol{\Theta},T}\underline{\boldsymbol{\eta}}_T \cdot (\boldsymbol{x} - \boldsymbol{x}_T) \in \mathcal{P}^1(T)$. By (44), we have $\boldsymbol{P}^0_{\boldsymbol{\Theta},T}\underline{\boldsymbol{\eta}}_T = \mathbf{grad}\,\phi_T = \mathbf{grad}\,\widetilde{\underline{I}^0_{U,T}\phi_T}$, and thus (49) with $\underline{v}_T = \underline{I}^0_{U,T}\phi_T$ yields

$$\begin{aligned}\|\boldsymbol{P}^0_{\boldsymbol{\Theta},T}\underline{\boldsymbol{\eta}}_T - \widetilde{\boldsymbol{\eta}}_T\|^2_{L^2(T)^2} &\lesssim \|\underline{\boldsymbol{G}}^0_T(\underline{I}^0_{U,T}\phi_T) - \underline{\boldsymbol{\eta}}_T\|^2_{\boldsymbol{\Theta},T}\\ &\lesssim \sum_{E\in\mathcal{E}_T} h_E\|\boldsymbol{P}^0_{\boldsymbol{\Theta},T}\underline{\boldsymbol{\eta}}_T\cdot\boldsymbol{t}_E - \boldsymbol{\eta}_E\cdot\boldsymbol{t}_E\|^2_{L^2(E)} \lesssim h_T^2\sum_{E\in\mathcal{E}_T} h_E^{-1}\|\boldsymbol{P}^0_{\boldsymbol{\Theta},T}\underline{\boldsymbol{\eta}}_T - \boldsymbol{\eta}_E\|^2_{L^2(E)},\end{aligned}$$

where the second inequality follows from the two-dimensional version of the norm equivalence [19, Eq. (4.24)] together with the local version of (10) which gives $\underline{\boldsymbol{G}}^0_T(\underline{I}^0_{U,T}\phi_T) = \underline{\boldsymbol{I}}^{\flat,0}_{\boldsymbol{\Theta},T}(\mathbf{grad}\,\phi_T) = \underline{\boldsymbol{I}}^{\flat,0}_{\boldsymbol{\Theta},T}(\boldsymbol{P}^0_{\boldsymbol{\Theta},T}\underline{\boldsymbol{\eta}}_T)$. The estimate (50) follows writing $h_T \le h$, summing over $T \in \mathcal{T}_h$, and invoking [20, Eq. (7.103) and (7.109)] to see that

$$\sum_{T\in\mathcal{T}_h}\sum_{E\in\mathcal{E}_T} h_E^{-1}\|\boldsymbol{P}^0_{\boldsymbol{\Theta},T}\underline{\boldsymbol{\eta}}_T - \boldsymbol{\eta}_E\|^2_{L^2(E)^2} \lesssim \|\mathsf{G}^0_{\mathrm{s},h}\underline{\boldsymbol{\eta}}_h\|^2_{L^2(\Omega)^{2\times2}} + |\underline{\boldsymbol{\eta}}_h|^2_{\mathrm{s,j},h}. \qquad \square$$

5 Numerical results

We illustrate the practical behaviour of the DDR scheme (25) on two different analytical solutions and three families of meshes of $\Omega = (0,1)^2$: (mostly) hexagonal meshes, triangular meshes, and locally refined meshes (with hanging nodes); Figure 1 shows a representative member of each family of meshes. The DDR tools and the scheme (for both clamped and simply supported boundary conditions) have been implemented in the `HArDCore2D` C++ framework (see `https://github.com/jdroniou/HArDCore`), which is based on linear algebra facilities from the `Eigen3` library (see `http://eigen.tuxfamily.org`). The resolution of the global sparse linear systems uses the `Intel MKL PARDISO` library (see `https://software.intel.com/en-us/mkl`). We focus on the h-convergence for the degrees $k \in \{0,1,2,3\}$, check the convergence rates, and discuss the robustness of the scheme with respect to the thickness t of the plate. In all the tests, the Young modulus is taken as $E = 1$, while the Poisson ratio is $\nu = 0.3$.

The error is computed as the (relative) $\|\cdot\|_{\boldsymbol{\Theta}\times U,h}$-norm of the difference between the approximate solution and the interpolate of the exact solution, that is:

$$E_h := \frac{\|(\underline{\boldsymbol{\theta}}_h - \underline{\boldsymbol{I}}^k_{\boldsymbol{\Theta},h}\boldsymbol{\theta}, \underline{u}_h - \underline{I}^k_{U,h}u)\|_{\boldsymbol{\Theta}\times U,h}}{\|(\underline{\boldsymbol{I}}^k_{\boldsymbol{\Theta},h}\boldsymbol{\theta}, \underline{I}^k_{U,h}u)\|_{\boldsymbol{\Theta}\times U,h}}.$$

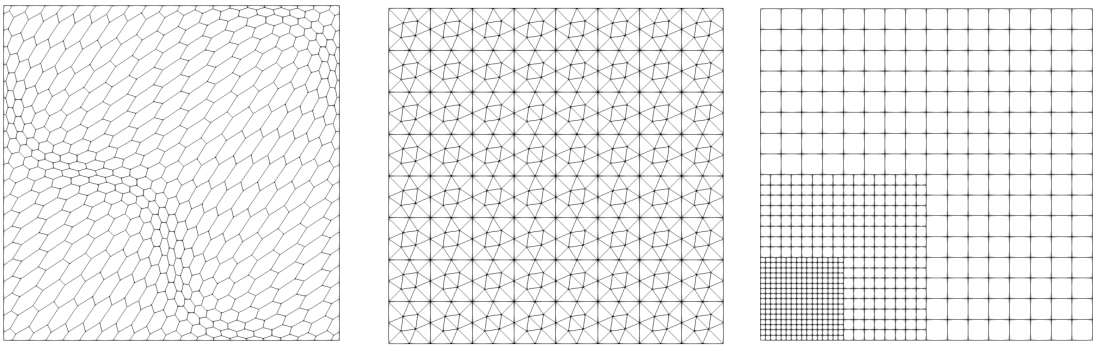

(a) Hexagonal mesh (b) Triangular mesh (c) Locally refined mesh

Figure 1: Members of mesh families used in numerical tests.

5.1 Polynomial solution

The first series of tests is run with source term corresponding to the following exact polynomial solution introduced in [17]:

$$
\begin{aligned}
u(\boldsymbol{x}) &= \frac{1}{3}x_1^3(1-x_1^3)x_2^3(1-x_2)^3 \\
&\quad - \frac{2t^2}{5(1-\nu)}\left[x_2^3(x_2-1)^3x_1(x_1-1)(5x_1^2-5x_1+1)+x_1^3(x_1-1)^3x_2(x_2-1)(5x_2^2-5x_2+1)\right], \\
\boldsymbol{\theta}(\boldsymbol{x}) &= \begin{bmatrix} x_2^3(x_2-1)^3x_1^2(x_1-1)^2(2x_1-1) \\ x_1^3(x_1-1)^3x_2^2(x_2-1)^2(3x_2-1) \end{bmatrix}.
\end{aligned}
$$

The results are presented in Figure 2. We notice that, for all considered polynomial degrees $k \in \{0,1,2,3\}$ and thicknesses $t \in \{10^{-1}, 10^{-3}\}$, the error decays as h^{k+1} (as expected from Theorem 4) and is mostly independent of t. The same observation can be made for $k \in \{0,1\}$ and $t = 10^{-5}$. However, for $k \geq 2$ we notice an apparent loss of convergence on the finest meshes when $t = 10^{-5}$.

This loss of convergence is actually not a sign of lack of robustness of the scheme, but rather a consequence of reaching the attainable precision combined with the accumulation of round-off errors. Indeed, the considered solution is such that the H^s-norms of the variables (displacement, rotation, shear strain) remain uniformly bounded with respect to t, and Theorem 4 thus shows that we should expect a convergence in $O(h^{k+1})$ with multiplicative constants that are independent of t. This apparent loss of convergence actually comes from unavoidable rounding errors. In double precision, the matrices of the local L^2-products $(\cdot,\cdot)_{\boldsymbol{\Theta},T}$ are typically computed with a precision in the range $[10^{-15}, 10^{-12}]$, the worst cases corresponding to higher polynomial degrees k and elements with many edges – situations in which the local L^2-products lead to the largest matrices. When these local matrices are multiplied by $t^{-2} = 10^{-10}$ (for $t = 10^{-5}$) to assemble the local term in b_h, the precision drops to $[10^{-5}, 10^{-2}]$. Due to this large scaling t^{-2}, the final precision on the global matrix is then rather poor, especially on meshes with a high number of elements; this poor precision prevents an accurate calculation of the approximate solution $(\underline{\boldsymbol{\theta}}_h, \underline{u}_h)$.

We notice that the tests we present here are among the few on high-order schemes for the Reissner–Mindlin plate model. In [9], isogeometric schemes are considered up to a polynomial degree 5, corresponding to a convergence rate in h^4, and thus to the choice $k = 3$ in the DDR scheme. The smallest thickness considered in this reference is $t = 10^{-3}$, and the largest mesh has about 300 rectangles; at these levels, no rounding error is noticeable in our tests (to compare, the second locally refined mesh we consider has more than 600 elements, and the largest one has more than 10,000 elements). An over-penalised discontinuous Galerkin scheme is presented in [14], and tests are produced with a polynomial

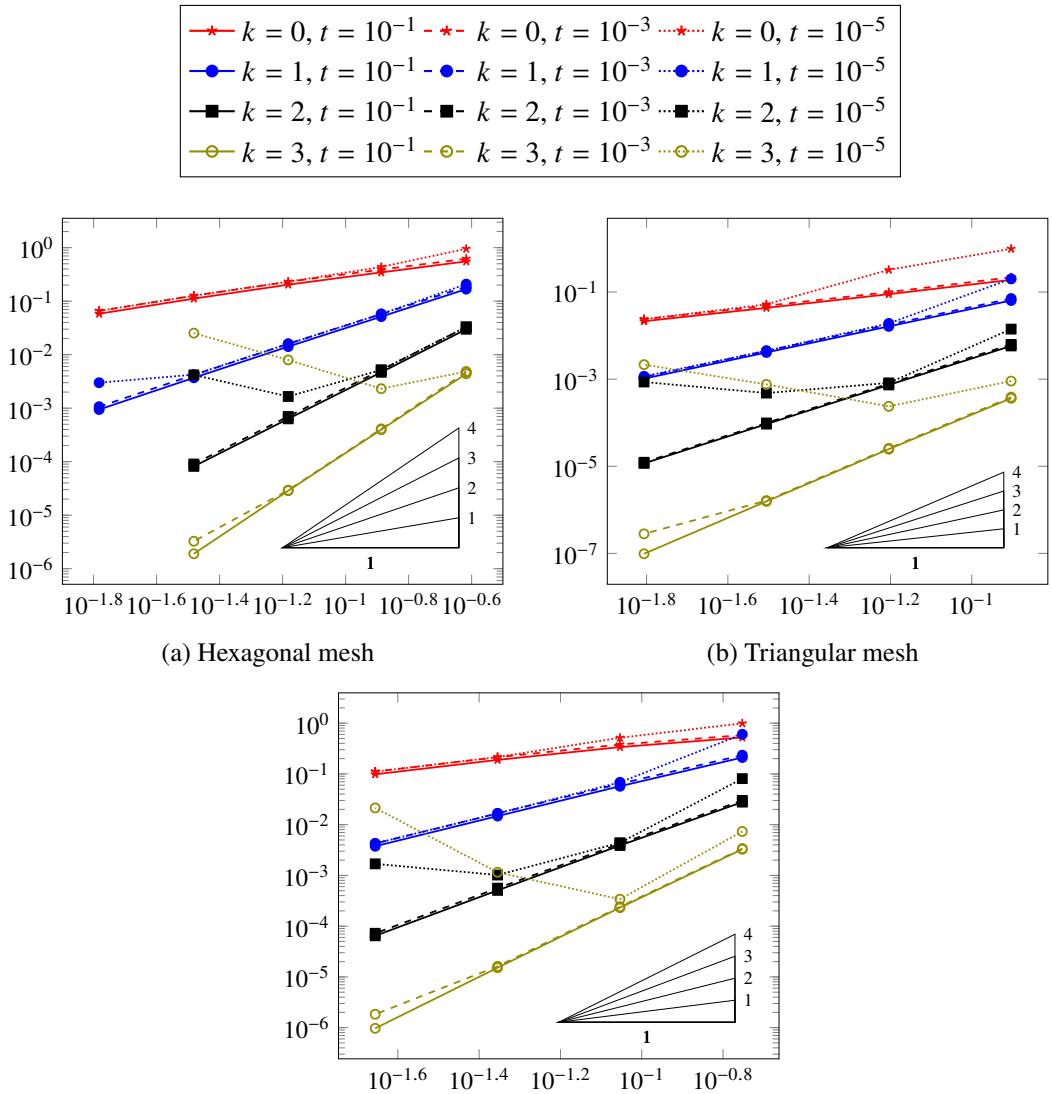

(a) Hexagonal mesh

(b) Triangular mesh

(c) Loc. Refined mesh

Figure 2: Error E_h w.r.t. h for the polynomial solution of Section 5.1.

degree 4 (convergence rate in h^3), corresponding to $k = 2$ for the DDR scheme. Very thin plates are considered in these tests, with t as small as 10^{-6}; however, for this thickness, the largest triangular mesh in the tests of [14] has 512 triangles; our second coarsest triangular mesh has 896 triangles and, as can be seen in Figure 2b, for $k = 2$ and at this size of mesh the convergence is not affected by round-off errors. It therefore seems that those previous tests were carried out under conditions in which round-off errors are not perceptible, and that the tests we present here are the first ones to highlight this phenomenon for high-order schemes and very thin plates.

5.2 Analytical solution with improved physical behaviour

As explained in [5, Theorem 2.1 and following remarks], as $t \to 0$ the shear strain $\boldsymbol{\gamma}$ is expected to remain bounded in L^2-norm, but to grow unboundedly in H^1-norm. The polynomial solution considered in Section 5.1 does not reproduce this behaviour (for this solution, the shear strain is actually independent of t). To test our DDR scheme in a setting which is at least quantitatively closer to the generic physical behaviour of the Reissner–Mindlin model, we design in this section a new analytical solution

on $\Omega = (0,1)^2$ (with non-homogeneous boundary conditions), with the following behaviour as $t \to 0$:

$$\|u\|_{H^3(\Omega)} \sim 1,\ \|\boldsymbol{\theta}\|_{H^2(\Omega)^2} \sim 1,\ \|\boldsymbol{\gamma}\|_{L^2(\Omega)^2} \sim 1,\ |\boldsymbol{\gamma}|_{H^s(\Omega)^2} \sim t^{-s+\frac{1}{2}} \text{ for all } s \geq 1, \quad \text{and } f \text{ is independent of } t. \tag{57}$$

As noticed in [5, Theorem 2.1], the expected growth of $|\boldsymbol{\gamma}|_{H^1(\Omega)}$ is in t^{-1}, not $t^{-\frac{1}{2}}$ as in the solution we construct here. This solution could easily be adjusted to produce such a growth, but this would come at the cost of extremely steep dependency on t (in particular, a term t^6 in (58) below) that would make the solution even more challenging to handle using double-precision arithmetic.

5.2.1 Design of the solution

We look for a solution under the form

$$u(\boldsymbol{x}) = v(t,\boldsymbol{x}) + t^2 w(t,\boldsymbol{x}) \text{ and } \boldsymbol{\theta}(\boldsymbol{x}) = \mathbf{grad}\, v(t,\boldsymbol{x}), \quad \text{where } v(t,\boldsymbol{x}) = t^3 V(t^{-1}\boldsymbol{x}) + g(\boldsymbol{x}) \text{ with } V(\boldsymbol{y}) = y_1 e^{-y_1}\cos(y_2) \text{ and } g(\boldsymbol{x}) = \sin(\pi x_1)\sin(\pi x_2). \tag{58}$$

Defining $\boldsymbol{\gamma}$ by (1c) gives $\boldsymbol{\gamma}(t,\cdot) = \kappa\, \mathbf{grad}\, w(t,\cdot)$. The function w is then selected to ensure that (1a) holds. Since $\mathbf{div}(\mathbf{C}\,\mathbf{grad}_{\mathrm{s}}\,\boldsymbol{\theta}) = \mathbf{div}(\mathbf{C}\,\mathbf{grad}_{\mathrm{s}}(\mathbf{grad}\, v)) = (\beta_0+\beta_1)\,\mathbf{grad}\,\Delta v$, (1a) corresponds to

$$w(t,\cdot) = -\frac{\beta_0+\beta_1}{\kappa}\Delta v(t,\cdot).$$

The transverse load f is fixed according to (1b):

$$f(t,\cdot) = (\beta_0+\beta_1)\Delta^2 v(t,\cdot).$$

Let us now briefly check that (57) holds. We first notice that, for any natural numbers m, n, the mapping $(0,\infty)\times\Omega \ni (t,\boldsymbol{x}) \mapsto (\partial_1^m\partial_2^n V)(t^{-1}\boldsymbol{x})$ is uniformly bounded. This shows that $\|u\|_{H^3(\Omega)}$, $\|\boldsymbol{\theta}\|_{H^2(\Omega)^2}$ and $\|\boldsymbol{\gamma}\|_{L^2(\Omega)^2}$ remain bounded as $t \to 0$; these norms also do not go to zero owing to the presence of g (which could actually be any smooth function with non-zero derivatives up to order 3). The function V satisfies $\Delta V(\boldsymbol{y}) = -2e^{-y_1}\cos(y_2)$ and thus $\Delta^2 V = 0$; hence, $f = (\beta_0+\beta_1)\Delta^2 g$ is independent of t. This also shows that

$$\boldsymbol{\gamma}(\boldsymbol{x}) = -2(\beta_0+\beta_1)e^{-t^{-1}y_1}\begin{bmatrix}\cos(t^{-1}y_2)\\ \sin(t^{-1}y_2)\end{bmatrix} - (\beta_0+\beta_1)\,\mathbf{grad}\,\Delta g(\boldsymbol{x}).$$

For a given $s \geq 1$, taking any partial derivative of order s of this expression and using $\|e^{-t^{-1}\bullet}\|_{L^2(0,1)} \sim t^{1/2}$ shows that $|\boldsymbol{\gamma}|_{H^s(\Omega)^2} \sim t^{-s+\frac{1}{2}}$.

5.2.2 Results

The results of the numerical tests with the analytical solution (58) are presented in Figure 3. We observe a similar behaviour as in the numerical results for the polynomial solution (see Figure 2). The scheme is here completely robust for $k = 0$ (as expected from Theorem 6), and for $k = 1$ up to $t = 10^{-3}$ (and also for $t = 10^{-5}$ up to errors of magnitude 10^{-3}). The degradation of convergence occurs however sooner, with respect to increasing k or $1/t$, than in Section 5.1: the apparent loss of convergence is here already perceptible for $(k,t) = (1, 10^{-5})$ or $(k,t) = (3, 10^{-3})$ for example; it also seems more severe for $t = 10^{-5}$ and $k \geq 1$.

This is not completely unexpected as the dependency of the analytical solution (58) with respect to t is more severe, and the higher-order norms of the shear strain indeed grows with t here. Combined with the round-off errors phenomenon previously mentioned, this explains the worse numerical behaviour. We however notice that the scheme remains more robust, even for higher degrees, than what the error estimate (32) could lead us to believe; considering for example $k = 3$, since $|\boldsymbol{\gamma}|_{H^4(\mathcal{T}_h)}$ grows as $t^{-3.5}$, the upper bound on the error in (32) grows between $t = 10^{-1}$ and $t = 10^{-3}$ by a factor $10^{2\times 3.5} = 10^7$, which is clearly not the case of the error itself (on the finest mesh, the ratio of the errors for these two values of t is at most 10^3).

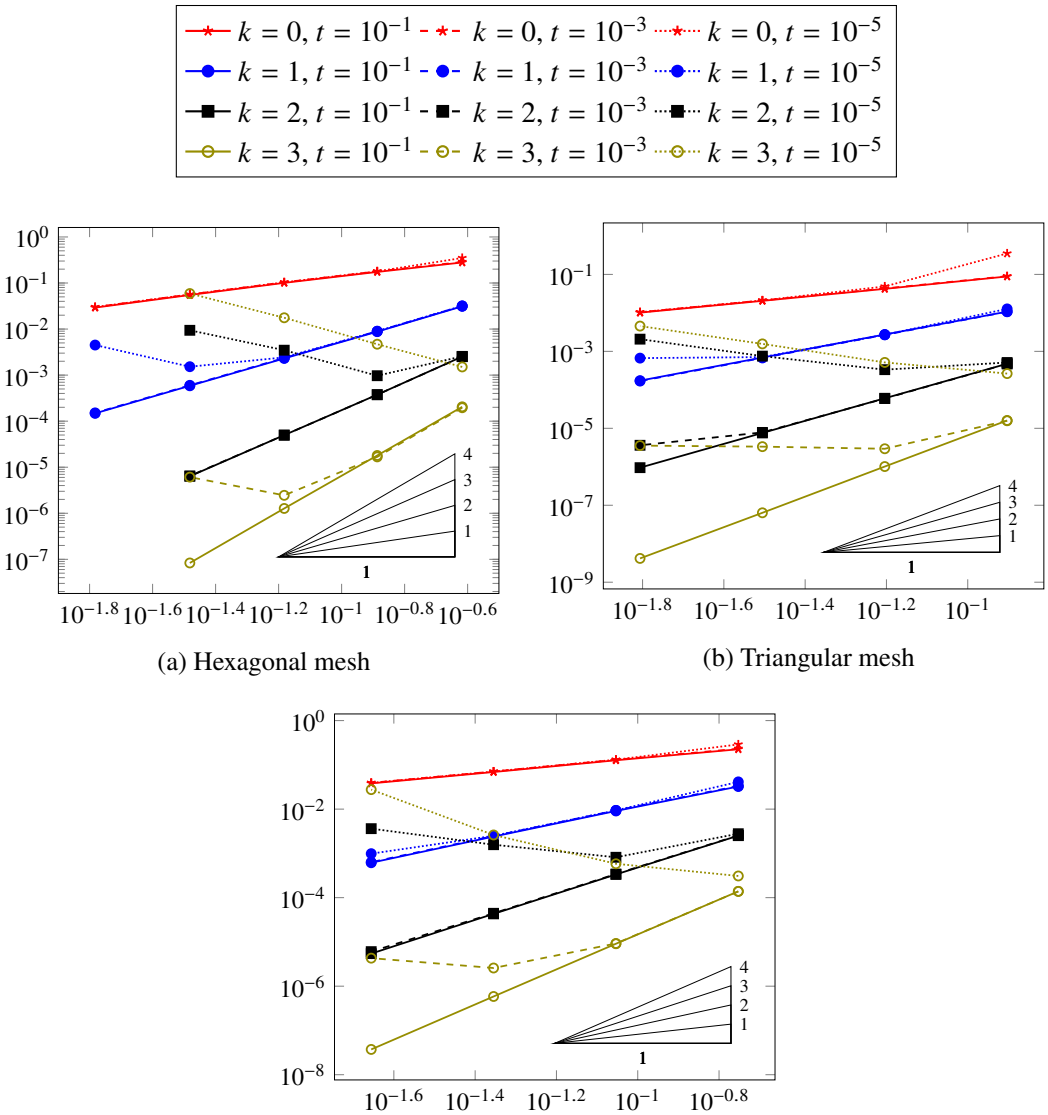

(a) Hexagonal mesh

(b) Triangular mesh

(c) Loc. Refined mesh

Figure 3: Error E_h w.r.t. h for the analytical solution of Section 5.2.

Acknowledgements

The authors acknowledge the partial support of *Agence Nationale de la Recherche* grant NEMESIS (ANR-20-MRS2-0004).

References

[1] P. F. Antonietti, S. Giani, and P. Houston. "hp-version composite discontinuous Galerkin methods for elliptic problems on complicated domains". In: *SIAM J. Sci. Comput.* 35.3 (2013), A1417–A1439. DOI: 10.1137/120877246.

[2] D. N. Arnold and F. Brezzi. "Some new elements for the Reissner-Mindlin plate model". In: *Boundary value problems for partial differential equations and applications*. Vol. 29. RMA Res. Notes Appl. Math. Masson, Paris, 1993, pp. 287–292.

[3] D. N. Arnold, F. Brezzi, R. S. Falk, and L. D. Marini. "Locking-free Reissner-Mindlin elements without reduced integration". In: *Comput. Methods Appl. Mech. Engrg.* 196.37-40 (2007), pp. 3660–3671. DOI: 10.1016/j.cma.2006.10.023.

[4] D. N. Arnold, F. Brezzi, and L. D. Marini. "A family of discontinuous Galerkin finite elements for the Reissner-Mindlin plate". In: *J. Sci. Comput.* 22/23 (2005), pp. 25–45. DOI: 10.1007/s10915-004-4134-8.

[5] D. N. Arnold and R. S. Falk. "A uniformly accurate finite element method for the Reissner-Mindlin plate". In: *SIAM J. Numer. Anal.* 26.6 (1989), pp. 1276–1290. DOI: 10.1137/0726074.

[6] D. N. Arnold and R. S. Falk. "Analysis of a linear-linear finite element for the Reissner-Mindlin plate model". In: *Math. Models Methods Appl. Sci.* 7.2 (1997), pp. 217–238. DOI: 10.1142/S0218202597000141.

[7] F. Bassi, L. Botti, A. Colombo, D. A. Di Pietro, and P. Tesini. "On the flexibility of agglomeration based physical space discontinuous Galerkin discretizations". In: *J. Comput. Phys.* 231.1 (2012), pp. 45–65. DOI: 10.1016/j.jcp.2011.08.018.

[8] F. Bassi, L. Botti, and A. Colombo. "Agglomeration-based physical frame dG discretizations: an attempt to be mesh free". In: *Math. Models Methods Appl. Sci.* 24.8 (2014), pp. 1495–1539. DOI: 10.1142/S0218202514400028.

[9] L. Beirão Da Veiga, T. J. R. Hughes, J. Kiendl, C. Lovadina, J. Niiranen, A. Reali, and H. Speleers. "A locking-free model for Reissner-Mindlin plates: analysis and isogeometric implementation via NURBS and triangular NURPS". In: *Math. Models Methods Appl. Sci.* 25.8 (2015), pp. 1519–1551. DOI: 10.1142/S0218202515500402.

[10] L. Beirão da Veiga and D. Mora. "A mimetic discretization of the Reissner-Mindlin plate bending problem". In: *Numer. Math.* 117.3 (2011), pp. 425–462. DOI: 10.1007/s00211-010-0358-8.

[11] L. Beirão da Veiga, D. Mora, and G. Rivera. "Virtual elements for a shear-deflection formulation of Reissner-Mindlin plates". In: *Math. Comp.* 88.315 (2019), pp. 149–178. DOI: 10.1090/mcom/3331.

[12] F. Bonaldi, D. A. Di Pietro, G. Geymonat, and F. Krasucki. "A Hybrid High-Order method for Kirchhoff–Love plate bending problems". In: *ESAIM: Math. Model Numer. Anal.* 52.2 (2018), pp. 393–421. DOI: 10.1051/m2an/2017065.

[13] P. R. Bösing and C. Carstensen. "Discontinuous Galerkin with weakly over-penalized techniques for Reissner-Mindlin plates". In: *J. Sci. Comput.* 64.2 (2015), pp. 401–424. DOI: 10.1007/s10915-014-9936-8.

[14] P. R. Bösing and C. Carstensen. "Weakly over-penalized discontinuous Galerkin schemes for Reissner-Mindlin plates without the shear variable". In: *Numer. Math.* 130.3 (2015), pp. 395–423. DOI: 10.1007/s00211-014-0672-7.

[15] F. Brezzi and M. Fortin. "Numerical approximation of Mindlin-Reissner plates". In: *Math. Comp.* 47.175 (1986), pp. 151–158. DOI: 10.2307/2008086.

[16] F. Brezzi, M. Fortin, and R. Stenberg. "Error analysis of mixed-interpolated elements for Reissner-Mindlin plates". In: *Math. Models Methods Appl. Sci.* 1.2 (1991), pp. 125–151. DOI: 10.1142/S0218202591000083.

[17] C. Chinosi, C. Lovadina, and L. D. Marini. "Nonconforming locking-free finite elements for Reissner-Mindlin plates". In: *Comput. Methods Appl. Mech. Engrg.* 195.25-28 (2006), pp. 3448–3460. DOI: 10.1016/j.cma.2005.06.025.

[18] D. A. Di Pietro and J. Droniou. "A third Strang lemma for schemes in fully discrete formulation". In: *Calcolo* 55.40 (2018). DOI: 10.1007/s10092-018-0282-3.

[19] D. A. Di Pietro and J. Droniou. *An arbitrary-order discrete de Rham complex on polyhedral meshes. Exactness, Poincaré inequalities, and consistency*. 2021. URL: https://arxiv.org/abs/2101.04940.

[20] D. A. Di Pietro and J. Droniou. *The Hybrid High-Order method for polytopal meshes. Design, analysis, and applications*. Modeling, Simulation and Application 19. Springer International Publishing, 2020. DOI: 10.1007/978-3-030-37203-3.

[21] D. A. Di Pietro and A. Ern. "A hybrid high-order locking-free method for linear elasticity on general meshes". In: *Comput. Meth. Appl. Mech. Engrg.* 283 (2015), pp. 1–21. DOI: 10.1016/j.cma.2014.09.009.

[22] D. A. Di Pietro and R. Specogna. "An a posteriori-driven adaptive Mixed High-Order method with application to electrostatics". In: *J. Comput. Phys.* 326.1 (2016), pp. 35–55. DOI: 10.1016/j.jcp.2016.08.041.

[23] J. Droniou and L. Yemm. "Robust Hybrid High-Order method on polytopal meshes with small faces". In: (2021), 26p. URL: https://arxiv.org/abs/2102.06414.

[24] R. Durán and E. Liberman. "On mixed finite element methods for the Reissner-Mindlin plate model". In: *Math. Comp.* 58.198 (1992), pp. 561–573. DOI: 10.2307/2153202.

[25] D. Gallistl and M. Schedensack. "Taylor–Hood Discretization of the Reissner–Mindlin Plate". In: *SIAM J. Numer. Anal.* 59.3 (2021), pp. 1195–1217. DOI: 10.1137/20M1343397.

[26] B. P. Lamichhane. "Two simple finite element methods for Reissner-Mindlin plates with clamped boundary condition". In: *Appl. Numer. Math.* 72 (2013), pp. 91–98. DOI: 10.1016/j.apnum.2013.04.005.

[27] B. P. Lamichhane and M. H. Meylan. "A new MITC finite element method for the Reissner–Mindlin place problem based on a biorthogonal system". In: *ANZIAM J.* 58 (2017), pp. C1–C20. DOI: 10.21914/anziamh.v58i0.11754.

[28] C. Lovadina. "A low-order nonconforming finite element for Reissner-Mindlin plates". In: *SIAM J. Numer. Anal.* 42.6 (2005), pp. 2688–2705. DOI: 10.1137/040603474.

[29] E. Oñate, F. Zarate, and F. Flores. "A simple triangular element for thick and thin plate and shell analysis". In: *International Journal for Numerical Methods in Engineering* 37.15 (1994), pp. 2569–2582. DOI: 10.1002/nme.1620371505.

[30] M. Schedensack. "A new generalization of the P_1 non-conforming FEM to higher polynomial degrees". In: *Comput. Methods Appl. Math.* 17.1 (2017), pp. 161–185. DOI: 10.1515/cmam-2016-0031.